# Chapter 4

# Intermediate Vector Boson Physics

#### 4.1 Introduction

Because of its success in describing low energy phenomenology and its relative economy in the number of fundamental fields, the  $SU(3)_C \times SU(2)_L \times U(1)_Y$  theory of strong and electroweak interactions, based on the principle of non-abelian gauge invariance, has become the Standard Model (SM).  $SU(3)_C$  embodies the current theory of the strong interactions, Quantum Chromodynamics (QCD), and is deemed to be an unbroken symmetry of nature. The  $SU(2)_L \times U(1)_Y$  sector is the basis of the Standard Electroweak Model and is spontaneously broken at a mass scale  $v = (\sqrt{2}G_{\mu})^{-1/2} = 246$  GeV into  $U(1)_Q$ , the Abelian gauge group of electromagnetism.

The SM has been very successful phenomenologically. It has provided the theoretical framework for the description of a very rich phenomenology spanning a wide range of energies, from the atomic scale up to the Z boson mass,  $M_Z$ . It is being tested at the level of a few tenths of a percent, both at very low energies and at high energies [1, 2]. However, the SM has a number of shortcomings. In particular, it does not explain the origin of mass and the observed hierarchical pattern of fermion masses, and why there are three generations of quarks and leptons. It is therefore widely believed that at high energies, or in very high precision measurements, deviations from the SM will appear, signaling the presence of new physics.

In this chapter we discuss the potential of probing the electroweak sector of the SM at the Tevatron ( $\sqrt{s} = 1.8$  TeV to 2 TeV) using very large integrated luminosities ( $\int \mathcal{L} dt = 1, \dots 10 \text{ fb}^{-1}$ ). With recent advances in accelerator technology, Tevatron collider luminosities of  $\mathcal{L} = 10^{33}$  cm<sup>-2</sup>  $s^{-1}$  may become reality within the next few years [3], resulting in integrated luminosities of up to 10 fb<sup>-1</sup>/year. The electroweak physics potential with such large integrated luminosities is best illustrated by the expected event yields for W/Z and di-boson production which are listed in Table 4.1. The approximately 10 million  $W \to e\nu$  and the 700,000  $Z \to e^+e^-$  events (a similar number is expected in the muon channel) can be employed to measure the W mass and width,  $M_W$  and  $\Gamma_W$ , with very high precision (Section 2), and to extract information on parton distributions from the W boson decay lepton charge asymmetry. The Z boson decay lepton forward backward asymmetry,  $A_{FB}$ ,

Table 4.1: Expected W, Z and di-boson event yields at the Tevatron for an integrated luminosity of 10 fb<sup>-1</sup>. Standard CDF/DØ lepton trigger and identification cuts are imposed. In addition, a cluster transverse mass larger than 90 GeV/c<sup>2</sup> is required for  $W\gamma$  production, and  $m(ee\gamma) > 100$  GeV/c<sup>2</sup> for  $p\bar{p} \to Z\gamma$ ,  $Z \to e^+e^-$ . In both processes a  $\Delta R(e,\gamma) > 0.7$  cut is imposed. In WW production, a jet veto is imposed to reduce the  $t\bar{t}$  background, and both charged leptons are required to have  $|\eta(\ell)| < 1$ .

channel	number of events
$W + X, W \to e\nu,  \eta(e)  < 1.2$	$6.4\cdot 10^6$
$Z + X, Z \rightarrow e^+e^-$	$7.4\cdot10^5$
$W\gamma, W \to e\nu, E_T(\gamma) > 10 \text{ GeV},  \eta(\gamma)  < 2.4$	$4.8\cdot 10^3$
$Z\gamma, Z \to e^+e^-, E_T(\gamma) > 10 \text{ GeV},  \eta(\gamma)  < 2.4$	$1.5\cdot 10^3$
$Z\gamma, Z \to \bar{\nu}\nu, E_T(\gamma) > 40 \text{ GeV},  \eta(\gamma)  < 1$	$1.1 \cdot 10^3$
$W^+W^-, W \to \ell\nu,  \ell = e,  \mu$	500
$WZ, W \to \ell\nu, Z \to \ell^+\ell^-, \ell = e, \mu$	200
$ZZ, Z \to \ell^+\ell^-, \ell = e, \mu$	30

can be used to determine  $\sin^2\theta_{eff}^{lept}$  with high precision. Both the W mass and  $\sin^2\theta_{eff}^{lept}$  can be utilized to extract the Higgs boson mass,  $M_H$ , from electroweak one-loop corrections. The W and Z asymmetries are discussed in detail in Section 3 of this chapter. The transverse momentum distribution of the Z boson can be used to measure the strong coupling constant  $\alpha_s$  (Section 4) while the very large sample of W boson events can also be employed to search for rare W decays (Section 5) and novel CP violating interactions [4] (Section 6).

One of the most direct consequences of the  $SU(2)_L \times U(1)_Y$  gauge symmetry are the self-couplings of the W, Z and photon. A direct measurement of these vector boson couplings is possible through the study of pair and triple gauge boson production processes like  $p\bar{p} \to W^+W^-$ ,  $W\gamma$ ,  $Z\gamma$ , WZ and  $p\bar{p} \to W\gamma\gamma$ ,  $Z\gamma\gamma$ ,  $W^+W^-\gamma$ , etc.. For an integrated luminosity of 10 fb<sup>-1</sup> one expects, e.g., about 5,000  $W\gamma$ ,  $W \to e\nu$ , and approximately 1,500  $Z\gamma$ ,  $Z \to e^+e^-$ , events with a photon of  $E_T(\gamma) > 10$  GeV (see Table 4.1). The large number of expected di-boson events will make it feasible to study the three boson self-interactions in detail. In  $W\gamma$  production, Tevatron experiments can also search for the SM "radiation zero", which provides an additional powerful test of the gauge theory nature of the SM. Measuring the transverse momentum distribution of the  $W\gamma$  system provides a test of QCD. Quantum Chromodynamics predicts a  $p_T$  distribution of the  $W\gamma$  system which is considerably harder than that observed in W production. For integrated luminosities of 10 fb<sup>-1</sup> or more, Tevatron experiments might also offer a first glimpse at triple electroweak boson production [5]. Triple gauge boson production provides a chance to measure the quartic gauge boson couplings

directly.

The first and major goal of measuring the self-couplings of W and Z bosons will be a confirmation of the SM predictions. A precise and direct measurement of the trilinear and quartic couplings of the electroweak vector bosons and the demonstration that they agree with the SM would beautifully corroborate spontaneously broken, non-abelian gauge theories as the basic theoretical structure describing the fundamental interactions of nature. At the same time, such measurements may be used to probe for new physics. Since it is possible to build extensions of the SM where the quartic couplings are modified but not the three vector boson couplings [6], it is necessary to measure both the trilinear and the quartic couplings separately in order to completely determine the self-interactions of the electroweak vector bosons. Di-boson production is considered in Section 7. In Section 8 we present a brief survey of triple vector boson production and the relevant background processes.

Finally, our conclusions are presented in Section 9.

#### 4.2 W Mass and Width Measurement

#### 4.2.1 Preliminaries

The mass of the W boson,  $M_W$ , is a fundamental parameter of the SM. Direct, precision measurements of  $M_W$ , and of the top quark mass,  $M_{top}$ , provide an indirect constraint on the Higgs boson mass,  $M_H$ , via top quark and Higgs boson electroweak radiative corrections to  $M_W$ . The ultimate test of the SM may lie in the comparison of these indirect determinations of  $M_H$  with its direct observation at the Tevatron (for  $M_H < 130$  GeV; see Chapter 6), or the LHC.

At the Tevatron, the W mass is extracted from a fit to the W transverse mass,  $M_T^W$ , distribution which sharply peaks in the vicinity of  $M_W$ . From the data collected in Run 1a (19 pb<sup>-1</sup>), CDF finds [7]

$$M_W = 80.41 \pm 0.18 \,\text{GeV/c}^2.$$
 (4.1)

The DØ Collaboration has not published a final result of their W mass analysis yet. The current world average [1],

$$M_W^{\text{World}} = 80.26 \pm 0.16 \,\text{GeV/c}^2$$
 (4.2)

is dominated by the CDF measurement from Run 1a.

### 4.2.2 W Mass Measurement at a Superluminous Tevatron

In estimating the precision of  $M_W$  which one may expect at high integrated luminosities, it is important to note that, besides the theoretical errors from electroweak one loop corrections and higher order corrections which each contribute about 20 MeV/c<sup>2</sup> to the current uncertainty in  $M_W$ , the dominant systematic errors are determined from control datasets

(Z boson events,  $J/\psi$  events). One therefore expects that the uncertainties on the W mass originating from those sources will approximately scale as  $1/\sqrt{N}$ , where N is the number of events, the same scaling law which applies to statistical errors.

In order to reduce the theoretical errors, improved calculations of radiative corrections are essential. Recently, a complete calculation of radiative W and Z boson production and decay, including initial and final state bremsstrahlung, finite W/Z decay lepton masses, and finite W/Z width effects [8] has been carried out. This will make it possible to reduce the error associated with radiative corrections substantially in the future, although certain non-factorizable QED final state interaction effects in  $qg \to W(\to \ell\nu)q'$  and higher order QED corrections which have not been calculated yet could conceivably induce an additional error in  $M_W$  of  $\mathcal{O}(10 \text{ MeV/c}^2)$  [9].

Some systematic errors, such as those originating from the W  $p_T$  distribution, or from uncertainties in the structure functions, are quasi-theoretical in nature and are associated with the details of the production process. These errors do not necessarily scale like  $1/\sqrt{N}$ . Structure function effects are controlled in part through the measurement of the W asymmetry which will be discussed in Section 3 of this chapter. In the case of the W  $p_T$  spectrum, the  $Z^0$  transverse momentum distribution and a new theoretical calculation of W and Z production which includes soft gluon resummation effects and W/Z decays in a Monte Carlo approach (RESBOS) [10] are expected to provide appropriate checks and improved theoretical guidance, and will make it possible to substantially reduce the current uncertainty of 45 MeV/ $c^2$  in  $M_W$  associated with the  $p_T(W)$  distribution. Since the uncertainty in the ratio of the W and Z transverse momentum distributions is, independent of the details of the nonperturbative parameterization, only a few per cent [11], the error originating from the W  $p_T$  distribution is controlled by how well the Z boson transverse momentum distribution is measured.

Theoretical predictions of the W transverse mass distribution including soft gluon resummation (solid line) and at NLO in QCD (dashed line) are shown in Fig. 4.1. In contrast to the resummed W transverse mass spectrum, the  $M_T^W$  distribution is ill defined in the peak region at NLO in QCD, due to the singularity in the W transverse momentum distribution at  $p_T(W) = 0$ . To obtain the NLO result shown in Fig. 4.1, the transverse mass distribution for  $p_T(W) > p_T^{sep}$  and the  $M_T^W$  distribution integrating from zero  $p_T$  to  $p_T^{sep}$  were added. The NLO transverse mass distribution resulting from this procedure then depends explicitly on the value of  $p_T^{sep}$  chosen. Fixing  $p_T^{sep}$  by requiring that the total cross section at NLO and including resummation effects is the same, one obtains the dashed line in Fig. 4.1.

With increasing luminosity, the average number of interactions per bunch crossing,  $I_C$ , may become considerably larger than one. For a luminosity of  $\mathcal{L} = 10^{32}$  cm<sup>-2</sup> s<sup>-1</sup> ( $\mathcal{L} = 10^{33}$  cm<sup>-2</sup> s<sup>-1</sup>) and a bunch spacing of 395 ns (132 ns) at the Tevatron, one expects  $I_C \approx 3$  ( $I_C \approx 9$ ) [3]. Multiple interactions degrade the resolution of the missing transverse energy (see Chapter 9) and thus of the  $M_T^W$  distribution. This is demonstrated in Fig. 4.2 where we show the W transverse mass distribution for various values of  $I_C$ . Multiple interactions are seen to considerably broaden the  $M_T^W$  distribution and to shift the peak position by several GeV/ $c^2$ . From our simulations we find that the resolution of the  $M_T^W$  distribution degrades approximately like  $\sqrt{I_C}$ . The impact of multiple interactions on the projected uncertainty in the W mass,  $\Delta M_W$ , as a function of the integrated luminosity is illustrated

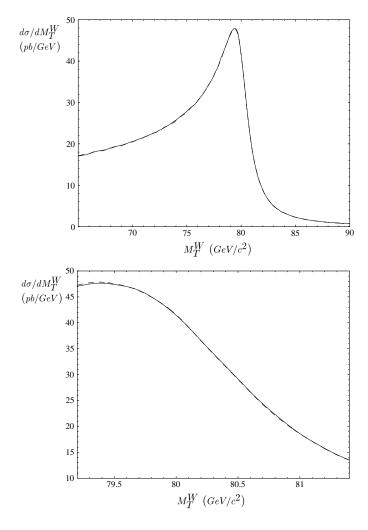


Figure 4.1: Distribution of the W transverse mass, at NLO (dashed line) and including soft gluon resummation effects (solid line) for  $p_T(\ell) > 25 \text{ GeV/c}$ ,  $\not E_T > 25 \text{ GeV}$ , and  $p_T(W) < 20 \text{ GeV/c}$  [7].

for the case  $I_C = 3$  in Fig. 4.3. To present graphically how 3 interactions per crossing affect the resolution of the transverse mass distribution, the scaling of the error on the mass reach is varied gradually such that it approaches the resolution for 3 interactions per crossing for 1 fb<sup>-1</sup>. For  $\int \mathcal{L}dt > 1$  fb<sup>-1</sup>, a fixed average number of  $I_C = 3$  interactions per crossing is assumed in this figure.

If one assumes that the theoretical uncertainties, due to calculational improvements such as those mentioned above, virtually also scale like  $\sqrt{I_C/N}$ , the total systematic error in  $M_W$  can be parameterized by

$$\Delta M_W|_{\rm sys} = (17.9 \text{ GeV/c}^2) \sqrt{\frac{I_C}{N}},$$
 (4.3)

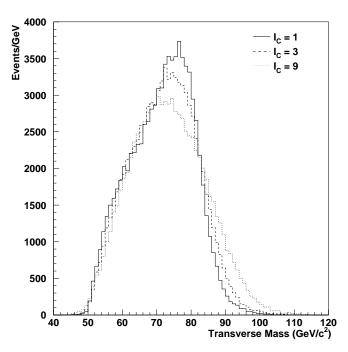


Figure 4.2: The effect of multiple interactions on the W transverse mass distribution. Standard kinematic cuts of  $p_T(e) > 25 \text{ GeV/c}$ ,  $|\eta(e)| < 1.2$ ,  $p_T > 25 \text{ GeV/c}$  and  $p_T(W) < 30 \text{ GeV/c}$  are imposed. The effect of multiple interactions is simulated by adding additional minimum bias events to the event containing the W boson.

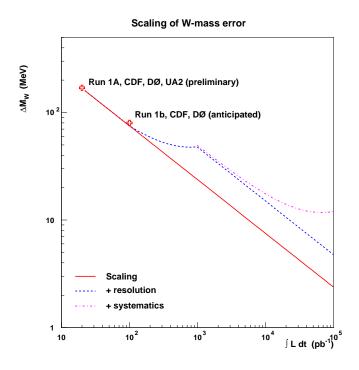


Figure 4.3: The effect of multiple interactions on the W mass uncertainty as a function of the integrated luminosity.

Table 4.2: Projected statistical and systematic errors (per experiment) on the W mass at the Tevatron, combining the  $W \to e\nu$  and  $W \to \mu\nu$  channel. Beneficial effects of the CDF and DØ upgrades for Run 2 are not included in the estimate.

$\Delta M_W$	$\int \mathcal{L}dt = 1 \text{ fb}^{-1}, I_C = 3$	$\int \mathcal{L}dt = 10 \text{ fb}^{-1}, I_C = 9$
statistical systematic	$29 \mathrm{\ MeV/c^2}$ $42 \mathrm{\ MeV/c^2}$	$17~\mathrm{MeV/c^2}$ $23~\mathrm{MeV/c^2}$
total	$51 \text{ MeV/c}^2$	$29 \text{ MeV/c}^2$

where N is the number of events. Similarly, the statistical uncertainty can be expressed as

$$\Delta M_W|_{\text{stat}} = (12.1 \text{ GeV/c}^2) \sqrt{\frac{I_C}{N}}$$
 (4.4)

The projected statistical and systematic errors per experiment, derived from Eqs. (4.3) and (4.4), for integrated luminosities of 1 fb<sup>-1</sup> and 10 fb<sup>-1</sup> are listed in Table 4.2. In order to obtain the normalization of Eqs. (4.3) and (4.4), we have combined the uncertainties of the  $W \to e\nu$  and  $W \to \mu\nu$  channels, using for definiteness the current efficiencies of CDF. This means that several beneficial effects of the CDF and DØ upgrades for Run 2 are not included in our estimate. The uncertainties in  $M_W$  listed in Table 4.2 will improve slightly by combining the results of CDF and DØ. Details, however, depend largely on which portion of the systematic errors will be common to both experiments in the future. This has not been studied yet and, therefore, we have not attempted to estimate the combined uncertainty.

For  $\mathcal{L}=10^{33}~\mathrm{cm^{-2}~s^{-1}}$ , multiple interactions are the dominating source of uncertainties in the W mass measurement. If one divides the total W sample into subsamples corresponding to a fixed number of interactions per crossing, it may be possible to reduce the negative effect of multiple interactions on  $\Delta M_W$ . Performing a separate fit to the W mass in each of the subsamples, one can study in detail how multiple interactions affect the resolution of the transverse mass distribution. This may then help to develop techniques to correct for the effect [12], and thus to achieve an ultimate uncertainty  $\Delta M_W$  considerably smaller than 29 MeV/c<sup>2</sup>. However, we have not explored this approach in detail yet.

Presently contemplated upgrades of the CDF and DØ detectors will allow for operation with a bunch spacing of 132 ns. As described in Ref. [3], bunch separations of as low as 19 ns are possible for  $\mathcal{L} = 10^{33}$  cm<sup>-2</sup> s<sup>-1</sup>. For a bunch spacing of 19 ns,  $I_C \approx 1$ , with a corresponding improvement in the uncertainty of  $M_W$  which one can hope to achieve. However, for such very short bunch separations, further detector upgrades, beyond those planned for Run 2, are necessary.

In summary, the values for  $\Delta M_W$  listed in Table 4.2 are expected to be realistic. As a benchmark, we assume in the following that the W boson mass can be determined with an uncertainty of  $\Delta M_W = 30 \text{ MeV/c}^2$  for  $\int \mathcal{L}dt = 10 \text{ fb}^{-1}$ . In view of the possibilities to improve the precision of the W mass measurement discussed above, however, a precision of

 $\Delta M_W = 20 \text{ MeV/c}^2$  may well be within reach.

In our discussion we have concentrated on the transverse mass distribution to extract  $M_W$ . As is clear from our discussion, the  $E_T$  resolution will be the main effect in limiting the precision of future W mass measurements using the transverse mass distribution.  $M_W$  can also be determined from other quantities, such as the energy distribution [13] or the  $p_T$  spectrum of the charged W decay lepton. Both methods only require a measurement of the charged lepton four-momentum and are therefore independent of the missing transverse energy resolution. However, in contrast to the  $M_T^W$  spectrum, the lepton  $p_T$  and energy distributions are very sensitive to higher order QCD corrections, in particular resummation effects [10]. We have not studied the potential of measuring the W mass using the charged lepton energy and transverse momentum distributions in detail. However, using the results of Ref. [13] and assuming that the systematic errors scale as  $1/\sqrt{N}$ , we estimate that  $M_W$  could be measured with a precision of  $\sim 20$  MeV using the lepton energy distribution.

### 4.2.3 Comparison with LEP II and LHC

The uncertainties listed in Table 4.2 should be compared with the errors on  $M_W$  expected from other collider experiments. At LEP II,  $M_W$  is expected to be measured with an accuracy of 60 MeV/c² to 80 MeV/c² per experiment [14] from either direct reconstruction of WW events, or a threshold scan. Taking common errors into account, this results in a projected overall precision of  $\Delta M_W = 40$  MeV/c² at LEP II [15]. No detailed study on the prospects of measuring the W mass at the LHC exists at this time. In principle,  $M_W$  can be extracted from the transverse mass distribution at the LHC. However, the large average number of interactions per crossing ( $I_C \approx 20$  at design luminosity) severely degrades the resolution of the  $M_T^W$  distribution. In addition, due to the high trigger threshold of  $E_T > 40$  GeV for electrons [2, 1, 18], most  $W \to e\nu$  events have a large recoil energy, which increases the background from heavy flavor decays and jets faking electrons. Without performing a detailed study, it thus not clear how well the W mass can be measured at the LHC.

# 4.2.4 Physics Significance of the W Mass Measurement at an Upgraded Tevatron

As we have mentioned before, the results of a precise measurement of the W and the top quark mass can be used to extract information on the Higgs boson mass which can then be confronted with the results of a direct search at the Tevatron or the LHC. This is illustrated in Fig. 4.4 which displays the results of the direct  $M_W$  and  $M_{top}$  measurements at the Tevatron with 10 fb<sup>-1</sup> in the  $(M_{top}, M_W)$  plane [20], assuming that the W mass (top quark mass) can be measured with a precision of 30 MeV/c² (2 GeV/c² [see Chapter 3]) and that the current central values of  $M_W$  and  $M_{top}$  will not change. The cross hatched bands show the SM prediction for the indicated Higgs boson masses. The width of the bands is due primarily to the uncertainty in the electromagnetic coupling constant at the Z mass scale,  $\alpha(M_Z)$ , which has been assumed to be  $\delta\alpha(M_Z) = 0.0004$ . Recent estimates of the uncertainty in  $\alpha(M_Z)$  give  $\delta\alpha(M_Z) \approx 0.0004 - 0.0007$  [21]. Future measurements at Novosibirsk, Daphne and Beijing, combined with theoretical progress, may well lead to a

# $M_W$ vs. $M_{top}$ 80.9 $10 \text{ fb}^{-1} \text{ data}, \sqrt{s} = 2 \text{ TeV}$ 80.8 $M_W = 80.260 \pm 0.030 \; GeV/c^2$ 80.7 $M_{top} = 176.0 \pm 2.0 \text{ GeV/c}^2$ $M^{M} (Ge^{N/c^{2}})$ 80.08 $M^{M}$ 80.09 Higgs Moss (GeV/c2) 80.3 80.2 80.1 180 190 210 $M_{top} (GeV/c^2)$

Figure 4.4: Expected results of a direct W and top quark mass measurement at the Tevatron with 10 fb<sup>-1</sup> versus SM predictions for various Higgs boson masses in the  $(M_{top}, M_W)$  plane, assuming that the current central values of  $M_W$  and  $M_{top}$  will not change. For the W mass, the current World average, and for  $M_{top}$  the present CDF central value are taken for definiteness. The theoretical predictions are based on the results of Ref. [19] and incorporate the effects of higher order electroweak and QCD corrections to  $\Delta \rho$  and  $\Delta r$ .

reduction in the error of  $\alpha(M_Z)$  of up to a factor 2. For the anticipated precision in  $\delta\alpha(M_Z)$ ,  $M_W$  and  $M_{top}$ , the Higgs boson mass can be predicted with an accuracy of approximately

$$M_{H - (1-f^{-1})M_{H}}^{+(f-1)M_{H}} \tag{4.5}$$

with  $f \approx 1.5$  [20]. This is illustrated in Fig. 4.5 which shows the theoretical expectations for the W mass versus the Higgs boson mass for  $M_{top} = 176.0 \pm 2.0 \text{ GeV/c}^2$ . A W mass measurement of  $M_W = 80.260 \pm 0.030 \text{ GeV/c}^2$  would constrain the Higgs boson mass to  $M_H = 685^{+355}_{-230} \text{ GeV/c}^2$ . The corresponding log-likelihood function of the electroweak one-loop corrections to  $M_W$  is shown in Fig. 4.6. If the W mass can be determined with a precision of 20 MeV/c<sup>2</sup>, a somewhat smaller error on the Higgs boson mass is obtained:  $M_H = 685^{+245}_{-180} \text{ GeV/c}^2$ . From Fig. 4.5 it is obvious that the Higgs boson mass obtained from a fit of the data to the SM electroweak radiative corrections depends very sensitively on the W boson mass. For example, from a measurement of  $M_W = 80.330 \pm 0.020 \text{ GeV/c}^2$ , one would obtain  $M_H = 285^{+105}_{-80} \text{ GeV/c}^2$ .

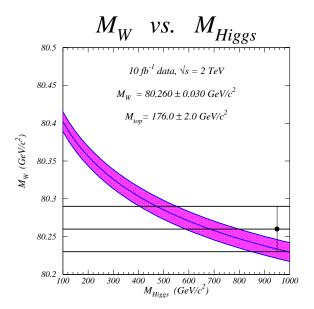


Figure 4.5: Predicted W versus Higgs boson mass for  $M_{top} = 176.0 \pm 2.0 \text{ GeV/c}^2$ . The theoretical predictions are based on the results of Ref. [19] and incorporate the effects of higher order electroweak and QCD corrections to  $\Delta \rho$  and  $\Delta r$ .

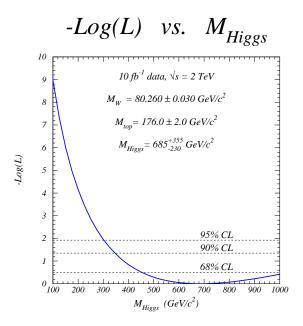


Figure 4.6: The negative log-likelihood function for  $M_W = 80.260 \pm 0.030 \text{ GeV/c}^2$  and  $M_{top} = 176.0 \pm 2.0 \text{ GeV/c}^2$ . The theoretical predictions are based on the results of Ref. [19] and incorporate the effects of higher order electroweak and QCD corrections to  $\Delta \rho$  and  $\Delta r$ .

Table 4.3: Expected experimental uncertainties (per experiment) on  $\Gamma_W$  from a fit to the W transverse mass distribution in the electron channel at the Tevatron.

$\Delta\Gamma_W$	$\int \mathcal{L}dt = 1 \text{ fb}^{-1}, I_C = 3$	$\int \mathcal{L}dt = 10 \text{ fb}^{-1}, I_C = 9$
statistical	40 MeV	$13~{ m MeV}$
background	8 MeV	$5~{ m MeV}$
$p_T(W)$	$17 \mathrm{MeV}$	8 MeV
energy scale	$6~{ m MeV}$	$3~{ m MeV}$
electron energy resolution	$10~{ m MeV}$	8 MeV
$ \not\!\!E_T $ resolution	14 MeV	8 MeV
total	48 MeV	$20~{ m MeV}$

#### 4.2.5 W Width and Branching Fraction Measurements

An important cross-check of our understanding of electroweak radiative corrections is provided by a measurement of the W leptonic branching ratio  $B(W \to \ell \nu)$ ,  $\ell = e$ ,  $\mu$ , and the total W width,  $\Gamma_W$ . Deviations from the SM predictions would signal the presence of new decay modes of the W boson. If the new states involved couple predominantly to quarks with a coupling constant much smaller than  $\alpha_s$ , such particles are difficult to detect in other measured quantities such as the di-jet invariant mass distribution.

The total width of the W boson can be measured directly from the tail of the  $M_T^W$  distribution [22].  $B(W \to \ell \nu)$  can be extracted from the cross section ratio

$$R_{W/Z} = \frac{\sigma_W \cdot B(W \to \ell \nu)}{\sigma_Z \cdot B(Z \to \ell^+ \ell^-)} , \qquad (4.6)$$

using the theoretical production cross section ratio  $\sigma(p\bar{p} \to W)/\sigma(p\bar{p} \to Z)$  and the LEP measurement of the branching ratio  $B(Z \to \ell^+\ell^-)$ . Assuming that the partial decay width  $\Gamma(W \to \ell\nu)$  is given by the SM, the measured cross section ratio  $R_{W/Z}$  can then be turned into a second, independent, determination of  $\Gamma_W$  [23]. Presently, the uncertainty on the W width is about 85 MeV per experiment from the measurement of the cross section ratio [23], and 324 MeV from the direct determination using the transverse mass distribution [22].

The projected experimental uncertainties (per experiment) for  $\Gamma_W$  from a fit to the W transverse mass distribution in the electron channel, are summarized in Table 4.3 for integrated luminosities of 1 fb<sup>-1</sup> and 10 fb<sup>-1</sup>. A similar precision is expected to be achieved in the muon channel. For 10 fb<sup>-1</sup>, the overall accuracy of 10 MeV which one hopes to reach combining the electron and muon channels, and measurements from CDF and DØ, approaches the level of the electroweak radiative corrections to  $\Gamma_W$  [24].

With  $\int \mathcal{L}dt = 10 \text{ fb}^{-1}$ , the expected precision for the cross section ratio  $R_{W/Z}$  measured

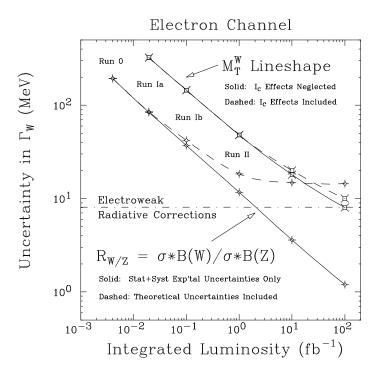


Figure 4.7: Projected uncertainty in  $\Gamma_W$  versus the integrated luminosity. The dot dashed line gives the absolute magnitude of the electroweak radiative corrections in the SM [24].

in the electron channel is,

$$\Delta R_{W/Z} = \pm 0.013 \text{ (stat.)} \pm 0.012 \text{ (exp. syst.)}$$
 (4.7)

which corresponds to an error in  $B(W \to e\nu)$  of  $\pm 1.8 \cdot 10^{-4}$ . This translates into a direct experimental uncertainty of  $\Delta\Gamma_W = \pm 3.4$  MeV, which is substantially better than what is expected from the direct measurement from the  $M_T^W$  spectrum. Unfortunately, the current theoretical error on the W/Z production cross section ratio,

$$\frac{\sigma(p\bar{p} \to W)}{\sigma(p\bar{p} \to Z)} = 3.358 \pm 0.020 \tag{4.8}$$

adds a systematic error of  $\Delta B(W \to e\nu) \approx 7.5 \cdot 10^{-4}$ , or  $\Delta \Gamma_W|_{\rm syst.} \approx 12$  MeV (the uncertainties from  $\Gamma(W \to \ell\nu)$  [theoretical] and  $B(Z \to \ell^+\ell^-)$  [LEP] are negligible compared to the error from  $\sigma(p\bar{p} \to W)/\sigma(p\bar{p} \to Z)$ ). The error on the production cross section ratio in Eq. (4.8) arises from uncertainties in the parton distributions, the value of  $\alpha_s$ , and higher order QCD corrections.

The expected precision for  $\Gamma_W$  in the electron channel (per experiment) versus the integrated luminosity is shown in Fig. 4.7. Effects from multiple interactions are seen to only marginally influence the W width measurement. For the current theoretical error from the production cross section ratio, the W width measurement from  $R_{W/Z}$  rapidly loses its power for integrated luminosities above 1 fb<sup>-1</sup>, and for  $\int \mathcal{L} dt > 20$  fb<sup>-1</sup> the direct measurement

from the  $M_T^W$  lineshape yields better results. Thus, in order to realize the full potential of the W width measurement from  $R_{W/Z}$ , the theoretical error on the production cross section ratio has to be reduced.

At LEP II,  $\Gamma_W$  can only be measured with a precision of about 400 MeV [25]. No studies for the LHC exist at this time.

Since the production cross section ratio in Eq. (4.8) is sensitive to the parton distributions,  $R_{W/Z}$  can in principle be used to discriminate between sets of parton distribution functions, if one assumes SM W and Z branching ratios. However, distributions which are sensitive to structure function effects, such as the triply differential di-jet distributions [26], or the same side – opposite side two jet ratio [27] contain more information than the single number resulting from a measurement of  $R_{W/Z}$  and are therefore expected to yield better constraints on the parton distributions.

## 4.3 Weak Boson Asymmetries

Uncertainties in the parton distribution functions (PDF's) are one of the major contributions to the error in the current W mass measurement [7]. The W charge asymmetry,

$$A(\eta_{\ell}) = \frac{d\sigma(W^{+})/d\eta_{\ell} - d\sigma(W^{-})/d\eta_{\ell}}{d\sigma(W^{+})/d\eta_{\ell} + d\sigma(W^{-})/d\eta_{\ell}}.$$
(4.9)

is a sensitive probe of the difference between u and d quark distributions, in particular of the slope of the d/u ratio versus x [28] at  $Q^2 = M_W^2$ . Here,  $\eta_\ell$  is the lepton pseudorapidity. The CDF measurement of  $A(\eta_\ell)$  in Run 1a [29] has demonstrated that the W charge asymmetry indeed provides a strong constraint on the PDF's. Recent fits [30] use the CDF data as an input when extracting the PDF's.

With very large integrated luminosities,  $A(\eta_{\ell})$  will be a very powerful discriminator between different sets of PDF's. In Fig. 4.8a, the W charge asymmetry is shown for two sets of parton distribution functions, together with the statistical uncertainties expected for 100 pb<sup>-1</sup> (MRSD-'), and 2 fb<sup>-1</sup> (CTEQ2M). The  $\sqrt{(\chi^2)}$  for CTEQ2M versus MRSD-' distributions, which is an estimate of the discriminating power of the W charge asymmetry between different sets of structure functions, is shown in Fig. 4.8b for the two integrated luminosities as a function of the maximum lepton rapidity. In order to fully utilize the sensitivity of the W charge asymmetry to the PDF's, a lepton pseudorapidity coverage out to  $|\eta^{\ell}|_{\text{max}} = 2.0$  is necessary. With an integrated luminosity of 100 pb<sup>-1</sup> (2 fb<sup>-1</sup>), a measurement with a significance of about  $10\sigma$  (50 $\sigma$ ) can be made. However, this does not mean that the uncertainty in  $M_W$  originating from the PDF's can be reduced by  $\sqrt{(\chi^2)}$ .  $A(\eta_{\ell})$  does not fully determine the parton distribution functions. For a complete determination it has to be supplemented by measurements of other quantities sensitive to the PDF's.

Since the lepton rapidity is not a singular quantity in W production, one naively expects that the NLO and the resummed calculations predict the same  $A(\eta_{\ell})$  distributions. However, once realistic lepton and  $E_T$  identification cuts are imposed, this is no longer true [10]. In a high precision measurement of PDF's from the W charge asymmetry it will be necessary to take these effects into account, as well as electroweak corrections.

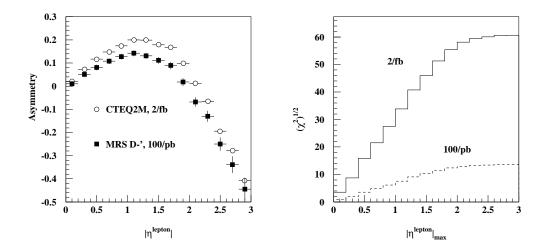


Figure 4.8: a) The predicted lepton charge asymmetry for W decays as a function of the lepton pseudorapidity. The error bars indicate the statistical uncertainty expected for 100 pb<sup>-1</sup> and 2 fb<sup>-1</sup>. b) The significance,  $\sqrt{(\chi^2)}$ , which results from a comparison of the MRSD-' and CTEQ2M sets of parton distributions, as a function of the pseudorapidity coverage of the detector.

The forward-backward asymmetry,  $A_{FB}$ , in  $p\bar{p} \to \ell^+\ell^-$  events arises from the parton level process  $q\bar{q} \to \ell^+\ell^-$ . This asymmetry depends on the vector and axial vector couplings of the quarks and leptons to the Z and is therefore sensitive to  $\sin^2\theta_{eff}^{lept}$ . The current combined error on  $\sin^2\theta_{eff}^{lept}$  from asymmetry measurements [1] at LEP and SLC is 0.00028.

The SM tree level prediction [31] for  $A_{FB}$  as a function of  $m(e^+e^-)$  for  $q\bar{q}\to e^+e^-$  is displayed in Fig. 4.9a for u and d quarks. The largest asymmetries occur at parton center-of-mass energies of around 70 GeV and above 110 GeV. The forward backward asymmetry as a function of the  $e^+e^-$  final state invariant mass in  $p\bar{p}\to e^+e^-$  at the Tevatron is shown in Fig. 4.9b. The error bars indicate the statistical errors for 100,000 events, corresponding to an integrated luminosity of about 2 fb<sup>-1</sup>. A preliminary study of the systematic errors, such as higher order electroweak corrections, indicates that most sources of error are small compared with the statistical error. The main contribution to the systematic error originates from unknown  $\mathcal{O}(\alpha^3)$  corrections and the uncertainty in the parton distribution functions – since the vector and axial vector couplings of u and d quarks to the Z are different, the measured asymmetry depends on the ratio of u to d quarks in the proton. Most of the systematic errors are expected to scale with  $1/\sqrt{N}$ , where N is the number of events. Using the rather conservative systematic errors of the existing CDF analysis of data taken in the 1988-89 run [32], we estimate the combined statistical and systematic error from the forward-backward asymmetry in the electron channel (per experiment) on  $\sin^2\theta_{eff}^{lept}$  to be

$$\pm 0.001 \text{ for } 1 \text{ fb}^{-1},$$
 (4.10)

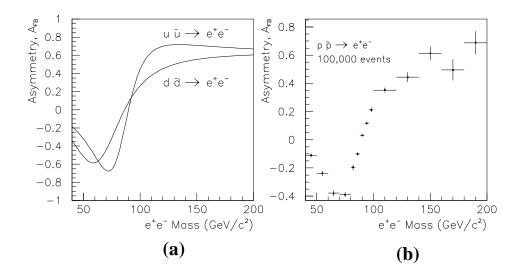


Figure 4.9: Forward-backward asymmetry as a function of  $e^+e^-$  invariant mass. (a) Standard Model tree level prediction for  $u\bar{u} \to e^+e^-$  and  $d\bar{d} \to e^+e^-$ ; (b) Simulation of  $p\bar{p} \to e^+e^-$  showing statistical errors for approximately 2 fb<sup>-1</sup>.

$$\pm 0.00032 \text{ for } 10 \text{ fb}^{-1},$$
 (4.11)

and

$$\pm 0.00010 \text{ for } 100 \text{ fb}^{-1}.$$
 (4.12)

It is found that most of the sensitivity of this measurement to  $\sin^2 \theta_{eff}^{lept}$  is at  $m(e^+e^-) \approx m_Z$  due to the strong variation of  $A_{FB}$  with  $\sin^2 \theta_{eff}^{lept}$  and the high statistics in this region. The expected precision of  $\sin^2 \theta_{eff}^{lept}$  in the electron channel (per experiment) versus the integrated luminosity is shown in Fig. 4.10, together with the combined current uncertainty from LEP and SLC experiments. A similar precision is expected in the muon channel.

Analogous to the W mass, a very high precision measurement of  $\sin^2\theta_{eff}^{lept}$  can be used to extract information on the Higgs boson mass [33]. This becomes clear from Fig. 4.11 which shows the theoretical expectation for  $\sin^2\theta_{eff}^{lept}$  as a function of the Higgs boson mass together with the precision expected for 10 fb<sup>-1</sup> in the electron channel. Here we have assumed  $M_{top}=176\pm 2~{\rm GeV/c^2}$ , an uncertainty of  $\delta\alpha(M_Z)=0.0004$  (see Section 2.4) and that the current central value of  $\sin^2\theta_{eff}^{lept}=0.23143$  [1] will not change. As we have mentioned above, the precision which can be achieved for  $\sin^2\theta_{eff}^{lept}$  is expected to be dominated by the statistical uncertainty. Combining the results of the electron and the muon channel, an overall uncertainty of 0.00023 for  $\sin^2\theta_{eff}^{lept}$  is expected. A measurement of  $\sin^2\theta_{eff}^{lept}=0.23143\pm0.00023$  would constrain the Higgs boson mass to  $M_H=415^{+225}_{-150}~{\rm GeV/c^2}$ .

The Higgs boson mass can thus be extracted with comparable accuracy from  $M_W$  and  $\sin^2 \theta_{eff}^{lept}$  for an integrated luminosity of 10 fb<sup>-1</sup>. While the determination of  $A_{FB}$  is in principle straightforward, the W mass measurement involves a number of unknown effects, like

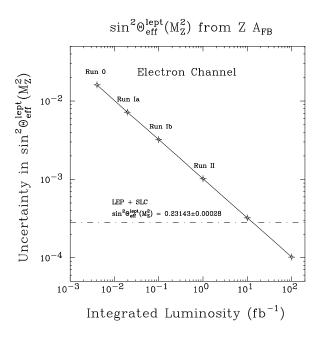


Figure 4.10: Projected uncertainty in  $\sin^2 \theta_{eff}^{lept}$  versus the integrated luminosity.

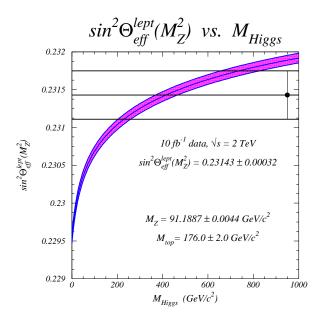


Figure 4.11: Predicted  $\sin^2 \theta_{eff}^{lept}$  versus the Higgs boson mass for  $M_{top} = 176.0 \pm 2.0 \text{ GeV/c}^2$ . The theoretical predictions are based on the results of Ref. [19] and incorporate the effects of higher order electroweak and QCD corrections to  $\Delta \rho$  and  $\Delta r$ .

pile-up effects. A measurement of  $\sin^2\theta_{eff}^{lept}$ , therefore, provides additional useful information on the Higgs boson mass. Since the systematic errors are very different for  $A_{FB}$  and the W mass measurement, it is straightforward to extract the expected precision on  $M_H$  from the combined measurement of the two variables. We find that  $M_W = 80.260 \pm 0.030 \text{ GeV/c}^2$  and  $\sin^2\theta_{eff}^{lept} = 0.23143 \pm 0.00023$  yield  $M_H = 540^{+185}_{-140} \text{ GeV/c}^2$ , i.e. the Higgs boson mass can be determined with an overall precision of  $\sim 30\%$ .

At the LHC, with 100 fb<sup>-1</sup>, a statistical error of  $\delta \sin^2 \theta_{eff}^{lept} = 6 \cdot 10^{-5}$  is expected [33], using the  $Z \to \mu^+ \mu^-$  decay channel. However, in contrast to the Tevatron, the initial state is charge symmetric (pp collisions), which makes it more difficult to determine the forward backward asymmetry.

# 4.4 Determination of $\alpha_s$ from the Z Boson $p_T$ Distribution

Measurements of the coupling strength of the strong interaction,  $\alpha_s$ , and of its energy dependence are key issues in probing the SM. At present, a large number of  $\alpha_s$  measurements from  $e^+e^-$  annihilation, from deep inelastic scattering, hadron colliders and from heavy quarkonia exists [34]. The energies covered range from the  $\tau$  lepton mass to the Z boson mass. While the results from low and high energy data overall are consistent with each other, the value of  $\alpha_s(M_Z)$  extracted from low energy data is approximately  $2\sigma$  lower than that found from data collected at high energies [34]:

$$\alpha_s(M_Z) = 0.1140 \pm 0.0032$$
 at low energies, (4.13)

$$\alpha_s(M_Z) = 0.1212 \pm 0.0034$$
 at high energies. (4.14)

Future experiments at the Tevatron offer an excellent opportunity to perform precision measurements of the strong coupling constant. In inclusive jet production,  $\alpha_s$  can be extracted over a broad range of momentum transfers [35], whereas the Z boson transverse momentum distribution offer a possibility to measure  $\alpha_s(M_Z)$  directly. The Z boson transverse momentum can be reconstructed entirely from the four momentum vectors of the Z decay leptons. Consequently, the systematic errors are significantly smaller than in jet measurements, and the  $p_T(Z)$  distribution is an ideal candidate quantity for measuring  $\alpha_s(M_Z)$  [36].

Determining  $\alpha_s$  at a hadron collider differs significantly from measuring it at LEP. At a hadron collider, cross sections depend on the PDF's which themselves are associated with  $\alpha_s(M_Z)$  as an input parameter. In order to extract the strong coupling constant from future Tevatron experiments, one therefore needs parton distribution functions where  $\alpha_s$  can be varied. Fits to the PDF's with variable  $\alpha_s$  have recently become available [37].

In the simulations carried out, modified versions of the CTEQ2 and CTEQ3 structure functions with variable  $\alpha_s$  have been used. The Z boson  $p_T$  distribution was calculated using the results of Ref. [38] in the region  $p_T(Z) > 40$  GeV, where the perturbative result accurately describes the data [39]. The factorization and normalization scale in the calculation were chosen to be equal to the Z boson mass. Using the CTEQ3M set, which corresponds to  $\alpha_s(M_Z) = 0.112$ , as a reference set, we show in Fig. 4.12 the relative change in the integrated

cross section above a minimum Z boson transverse momentum,  $q_{T\min}$ , as a function of  $q_{T\min}$  for a variety of values for  $\alpha_s$ . From Fig. 4.12a one observes that the Z boson transverse momentum distribution is primarily sensitive to values of  $\alpha_s(M_Z) < 0.112$ . For values of  $q_{T\min}$  between 40 GeV and 60 GeV, the relative change in the cross section varies only slightly with  $q_{T\min}$ . The theoretical uncertainties originating from the choice of the renormalization scale are much smaller than those from varying  $\alpha_s$ . For  $\alpha_s(M_Z) < 0.112$ , the Z boson cross section is falling with the strong coupling constant, as expected from the parton level cross section formula. For  $\alpha_s(M_Z) > 0.112$ , on the other hand, the situation is more complicated. In this region the shape change in the PDF's for the CTEQ3 parameterization partly compensates the increase from the parton level cross section. In the CTEQ3 fit, the shape parameter is one of those variables which are determined from the fit to the data.

The shape change of the PDF's with the strong coupling constant depends rather sensitively on which parameterization is used. This is illustrated in Fig. 4.12b where the relative change of the cross section is shown for CTEQ2 parton distribution functions. Varying the parton distribution functions for constant  $\alpha_s$  produces a relative change of the cross section similar to that of varying  $\alpha_s(M_Z)$  from 0.107 to 0.120.

The inclusive  $Z \to e^+e^-$ ,  $\mu^+\mu^-$  production cross section for Z boson transverse momenta larger than 50 GeV is approximately 13 pb. For integrated luminosities of 1 fb<sup>-1</sup> or more, the cross section, therefore, can be measured with a statistical error smaller than 1%. The systematic errors are expected to be dominated by the luminosity uncertainty ( $\sim 3.6\%$ ) [40], the lepton energy scale ( $\sim 1\%$ ), the lepton energy resolution ( $\sim 1\%$ ), and the uncertainty of the angular resolutions. The luminosity uncertainty, which currently dominates, may be reduced substantially in the future by using the  $W \to e\nu$  and  $Z \to e^+e^-$  cross sections to determine the integrated luminosity. Alternatively, the cross section ratio  $\sigma_Z(q_T > q_{T\min})/\sigma_Z$ , where  $\sigma_Z$  is the total Z boson cross section can be used. The luminosity uncertainty cancels in the cross section ratio. The precision which can be achieved for  $\alpha_s(M_Z)$  will then crucially depend on how well the parton distribution functions can be determined in other experiments.

## 4.5 Rare W and Z Decays

With the copious number of leptonic W and Z decays to be collected in future Tevatron experiments, one can begin to look for rare W and Z decays. The number of  $Z \to e^+e^-$ ,  $\mu^+\mu^-$  events expected at the Tevatron with 10 fb<sup>-1</sup> is similar to that collected at LEP so far. Hence, one does not expect that the current limits on rare Z decays can be significantly improved in future Tevatron experiments, and we shall concentrate on rare W decays in the following. For a survey of rare Z decays we refer the reader to Ref. [41].

#### 4.5.1 Theoretical Overview

W decays into a pseudoscalar meson and a photon,  $W \to P\gamma$ , and two pseudoscalar mesons,  $W \to P_1 P_2$ , are particularly attractive. Decays into a pseudoscalar meson and a photon are sensitive to new physics which affects the  $WW\gamma$  vertex. A search for  $W \to P\gamma$  decays

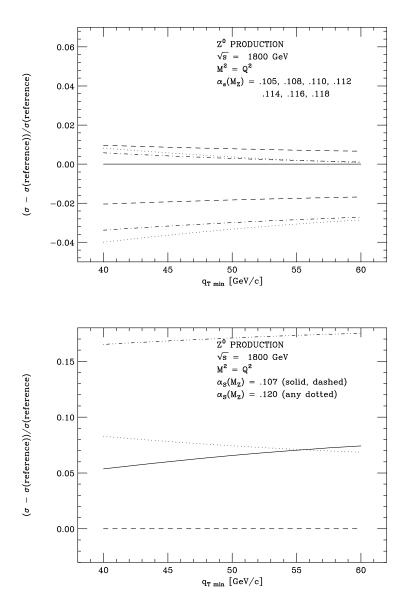


Figure 4.12: Relative change of the Z boson cross section above a minimum Z boson transverse momentum  $q_{T\min}$ , as a function of  $q_{T\min}$ . a) The solid line gives the result for the CTEQ3M set of parton distribution functions, which correspond to  $\alpha_s(M_Z) = 0.112$ . This set serves as a reference point. The upper (lower) dashed, dot-dashed and dotted lines correspond to  $\alpha_s(M_Z) = 0.114$  (0.110), 0.116 (0.108), and 0.118 (0.105). b) The relative change of the Z boson cross section for CTEQ2 PDFs with the same shape parameters for  $\alpha_s = 0.107$  (solid and dashed lines) and  $\alpha_s = 0.120$  (dotted and dot-dashed lines).

thus complements the di-boson analysis described in detail in Section 7. On the other hand,  $W \to P_1 P_2$  decays offer an opportunity to probe meson decay form factors at a very high momentum transfer where these form factors have not been tested so far. Currently, experimental results exist only for the decay  $W \to \pi \gamma$  [42, 43].

The  $W \to P\gamma$  decay rate can be expressed in terms of one vector and one axial vector form factor [44],

$$\frac{\Gamma(W \to P\gamma)}{\Gamma(W \to \ell\nu)} = \frac{1}{4} \alpha \pi |V_{ij}|^2 \left( |V_P(M_W^2)|^2 + |A_P(M_W^2)|^2 \right) M_W^2 \left( 1 - \frac{m_P^2}{M_W^2} \right)^3. \tag{4.15}$$

Here,  $V_P$  and  $A_P$  are the vector and axial vector form factor, respectively,  $m_P$  is the mass of the pseudoscalar meson P, and  $V_{ij}$  is the relevant quark mixing matrix element.

In all cases of interest, the mass of the pseudoscalar meson is much smaller than the W mass. In this situation, the large momentum transfer behaviour of the vector form factor can be calculated from QCD [45]:

$$V_P(q^2) = -\frac{f_P}{q^2} (1 + \mathcal{O}(\alpha_s(q^2))) \quad \text{for} \quad q^2 \to \infty$$
 (4.16)

where  $q^2$  is the momentum transfer squared and  $f_P$  is the pseudoscalar decay constant. A detailed QCD analysis has not been carried out for the axial vector form factors so far. However, because the weak charged current is purely lefthanded, one expects that

$$\frac{A_P(q^2)}{V_P(q^2)} \to 1 \qquad \text{for} \qquad q^2 \to \infty. \tag{4.17}$$

The branching ratios for the  $W \to P\gamma$  decays calculated from Eqs. (4.15) – (4.17) are listed in Table 4.4. Here we have used

$$f_{\pi} = 132 \text{ MeV},$$
 (4.18)

$$f_K = 158 \text{ MeV}, \tag{4.19}$$

$$f_D = 210 \text{ MeV}, \tag{4.20}$$

$$f_{D_s} = 230 \text{ MeV}, \tag{4.21}$$

$$f_B = 190 \text{ MeV},$$
 (4.22)

$$f_{B_c} = 500 \text{ MeV}.$$
 (4.23)

The present theoretical uncertainties in the D,  $D_s$  and B decay constants are substantial, and experimental results indicate that the  $D_s$  decay constant could well be a factor 1.5 larger [46] than the value listed in Eq. (4.23). The value of  $f_{B_c}$  can rather accurately be predicted from potential models [47].

From Table 4.4 one observes that, in the SM, all  $W \to P\gamma$  decays are expected to have very small branching ratios. The  $W \to \pi\gamma$  and  $W \to D_s\gamma$  modes are predicted to be the most prominent  $W \to P\gamma$  decays. The CDF Collaboration has searched for  $W \to \pi\gamma$  in the 1988-89 and 1992-93 run and established a limit of  $BR(W \to \pi\gamma) < 2 \times 10^{-4}$  (95% CL) [42].

Table 4.4: Branching ratios of rare W decays in the SM. The branching ratios for decays into two pseudoscalars are obtained in the nearest pole model (see Eq. (4.24)) with  $f_+^{\pi^+\pi^0}(0) = \sqrt{2}$ ,  $f_+^{K\pi}(0) = 1.37$ , and  $f_+^{DK}(0) = 0.75$  (see Ref. [48]). In all other cases we use  $f_+^{P_1P_2}(0) = 1$ .

mode	br. ratio	mode	br. ratio
$W \to \pi \gamma$	$3.3 \cdot 10^{-9}$	$W \to \pi\pi$	$2.2 \cdot 10^{-10}$
$W \to K \gamma$	$2.4 \cdot 10^{-10}$	$W \to K\pi$	$2.0 \cdot 10^{-11}$
$W \to D\gamma$	$3.4 \cdot 10^{-10}$	$W \to D\pi$	$2.3 \cdot 10^{-10}$
$W \to D_s \gamma$	$1.0 \cdot 10^{-8}$	$W \to DK$	$4.1 \cdot 10^{-9}$
$W \to B\gamma$	$7.1 \cdot 10^{-14}$	$W \to B\pi$	$3.6 \cdot 10^{-12}$
$W \to B_c \gamma$	$7.7 \cdot 10^{-11}$	$W \to BD$	$1.2 \cdot 10^{-9}$

The rate for the decay of a W boson into two pseudoscalar mesons  $P_1$  and  $P_2$  can be expressed in terms of the  $P_1 \to P_2 \ell \nu$  decay form factor  $f_+^{P_1 P_2}(q^2)$ , where  $P_1$  is the heavier of the two pseudoscalar mesons. Assuming  $m_{P_1}$ ,  $m_{P_2} \ll M_W$ , one finds:

$$\Gamma(W \to P_1 P_2) = \frac{G_F}{\sqrt{2}} \frac{M_W^3}{48\pi} |V_{ij}|^2 |f_+^{P_1 P_2}(M_W^2)|^2.$$
 (4.24)

In order to derive a numerical value for  $\Gamma(W \to P_1 P_2)$ , one needs to know  $f_+^{P_1 P_2}(M_W^2)$ . Presently, a QCD calculation of these form factors is not available and one has to rely on a simple model to make quantitative predictions. The available data from  $P_1 \to P_2 \ell \nu$  decays [46, 48] are consistent with a simple nearest pole model of the form

$$f_{+}^{P_1 P_2}(q^2) = f_{+}^{P_1 P_2}(0) \frac{m_V^2}{m_V^2 - q^2}$$
(4.25)

where  $m_V$  is the mass of the nearest vector meson with the appropriate quantum numbers  $(m_{\rho} \text{ for } f_{+}^{\pi^{+}\pi^{0}}, m_{K^{*}} \text{ for } f_{+}^{K\pi}, m_{D^{*}} \text{ for } f_{+}^{D\pi}, m_{B^{*}} \text{ for } f_{+}^{B\pi}, \text{ and } m_{B_{c}^{*}} \text{ for } f_{+}^{BD}).$  The branching ratios obtained with this ansatz are also listed in Table 4.4.

However, in  $P_1 \to P_2 \ell \nu$  the form factors are only measured for small momentum transfers of a few GeV<sup>2</sup> at most, which results in large uncertainties when they are extrapolated to  $q^2 = M_W^2$ . At small momentum transfer, one expects rather large non-perturbative contributions to the weak decay form factors. The pole model may thus well overestimate the  $W \to P_1 P_2$  rates and in W decays, *i.e.* at high momentum transfer, these effects should be absent [49]. On the other hand, it is not excluded that the nearest pole model underestimates the  $W \to P_1 P_2$  decay rates.

In conclusion, the numerical results listed in Table 4.4 should only be used as guidance. Presently, no reliable calculation of weak decay form factors at high  $q^2$  exists. A perturbative QCD calculation of these form factors similar to that of Ref. [45] is clearly warranted.

#### 4.5.2 Experimental Aspects

Within the context of the SM, from an experimental perspective, integrated luminosities of  $100 \text{ fb}^{-1}$  (or more) will be required in order to have any hope of observing even the most promising of these rare decay modes of the W boson listed in Table 4.4. Observation of any of these decay modes in significant excess of their SM predictions would certainly be exciting, and could be interpreted as an indicator of new physics beyond the SM, or a complete inadequate understanding of meson decay form factors. As mentioned already, W decays into two pseudoscalar mesons offer an opportunity to probe meson decay form factors at very high momentum transfer where these form factors have not been probed before. Hence searches for these and other rare decay modes of both the W and the Z are important to carry out whenever the opportunity exists.

For the rare decay  $W^{\pm} \to P^{\pm} \gamma$ , where  $P^{\pm}$  is a charged pseudoscalar meson, the dominant background at the Tevatron is due to photon + jet production, where the jet fragments to a single, leading charged particle, if  $P^{\pm} = \pi^{\pm}$  or  $K^{\pm}$ , or fragments to a low charged multiplicity jet, if  $P^{\pm} = D^{\pm}$ ,  $D_s^{\pm}$ ,  $B^{\pm}$ ,  $B_c^{\pm}$ . Although the photon + jet cross section is large, this background can be suppressed by the requirement of an isolated single high  $p_T$  charged track. Alternatively, a low multiplicity of isolated charged tracks, such that the invariant mass of photon+tracks is  $\sim M_W$  can be required. In addition, the  $p_T$  distributions of both daughter particles from W decay display the characteristic shape of a Jacobian peak at  $\sim M_W/2$ , whereas the background is steeply falling with  $p_T$ .

The current 95% CL experimental upper limit on the branching ratio for  $W^{\pm} \to \pi^{\pm} \gamma$  is  $BR(W^{\pm} \to \pi^{\pm} \gamma) < 2 \times 10^{-4}$  from 16.7 pb<sup>-1</sup> Run 1a CDF data [42]. The trigger for these events requires an isolated, high  $p_T$  photon in the central ( $|\eta| < 1$ ) region of the detector. No requirement is made at the trigger level for an additional isolated high  $p_T$  track, as this is not necessary. The mass resolution for photon + single charged track, each with a transverse momentum of  $\sim M_W/2 \sim 40$  GeV/c from W decay is excellent,  $\Delta M_W \sim 1.7$  GeV/c<sup>2</sup> ( $< \Gamma_{tot}^W \sim 2.1$  GeV). Hence the offline event selection required an isolated high  $p_T$  central photon and an isolated high transverse momentum central track within a  $\sim 4$  GeV/c<sup>2</sup> mass window centered on  $M_W$ . This selection reduces the background from photon+jet processes dramatically. One candidate event is observed within the mass window with an estimated background of  $2.6 \pm 1.0(stat) \pm 1.3(syst)$  events. The overall acceptance times efficiency for this W decay mode, for central photons and  $\pi^{\pm}$  is  $(6.0 \pm 0.2 \pm 0.7)\%$ .

With greatly increased integrated luminosity, it will be difficult to maintain a good signal/background ratio without substantially diminishing the overall  $W^{\pm} \to \pi^{\pm} \gamma$  detection efficiency by tightening up cuts used in the present analysis. Since the W boson has a natural width comparable to the size of the mass window used in the current analysis, narrowing the mass window will result only in a linear reduction in background, even if the mass resolution were substantially improved. Developing improved analysis methods for enhanced rejection of the single track background from the photon + jet "continuum" will be important if reductions in the experimental upper limit on this branching ratio are to be achieved.

An irreducible background to  $W^{\pm} \to \pi^{\pm} \gamma$  originates from the weak decay  $W \to q\bar{q}'$ , where the q and  $\bar{q}'$  jets fragment in such a way that a leading, single charged track from one jet mimics a  $\pi^{\pm}$ , and a leading  $\pi^0$  (or  $\eta$ ) from the other jet mimics a photon. In the present

CDF analysis, this background has been estimated to have an effective branching ratio of  $BR(W \to q\bar{q}' \to \pi^{\pm} + "\gamma") \sim 3 \times 10^{-8}$  (approximately one order of magnitude larger than the SM prediction for the  $W^{\pm} \to \pi^{\pm}\gamma$  signal and about two orders of magnitude higher than the SM prediction for the true two-body  $W^{\pm} \to \pi^{\pm}\pi^{0}$  process -c.f. Table 4.4).

If single track  $W^{\pm} \to P^{\pm} \gamma$  decays are observed, it will be difficult to distinguish a  $\pi^{\pm}$  with  $p_T \sim 40$  GeV/c from a  $K^{\pm}$ . Good particle identification, which works well in this momentum region is required. However, from the SM prediction of the ratio of branching ratios, we expect

$$\frac{BR(W^{\pm} \to K^{\pm} \gamma)}{BR(W^{\pm} \to \pi^{\pm} \gamma)} \simeq \frac{f_K^2 |V_{us}|^2}{f_{\pi}^2 |V_{ud}|^2} \sim 0.07, \tag{4.26}$$

hence  $W^{\pm} \to \pi^{\pm} \gamma$  is expected to dominate any observed photon + single track signal, within the context of the SM.

The rare W decays with single charged charm and/or B mesons in the final state have backgrounds from photon + charm (e.g.  $gc \to \gamma c$ ;  $q\bar{q} \to \gamma g$ ,  $g \to c\bar{c}$ ) and photon + b (e.g.  $gb \to \gamma b$ ,  $b \to c + X$ ;  $q\bar{q} \to \gamma g$ ,  $g \to b\bar{b}$ ) where the charm or b-jet fragments to a leading single charged charm or B meson, respectively. At  $\sqrt{\hat{s}} \sim M_W$ , these cross sections are known to be substantially less than the photon + light-quark jet cross section. Note also that the SM prediction for  $BR(W \to D_s \gamma)$  is the largest of this class of rare W decays.

The rare W decay modes  $W \to D(B)\gamma$  are suppressed by the quark mixing matrix element relative to  $W \to D_s(B_c)\gamma$ . Focusing on the charmed meson rare W decay modes (since these have the most favorable SM predictions), the all-charged 3-body decay modes of the D and  $D_s$  charmed mesons have branching fractions of  $BR(D^+ \to K^-\pi^+\pi^+) \sim 9.1\%$  and  $BR(D_s^+ \to K^+K^-\pi^+) \sim 4.8\%$ , respectively. Using these decay modes, a well-identified, isolated 3-prong secondary vertex requirement can be made using 3-D silicon microvertex information to reject light quark backgrounds, and suppress photon + charm and photon + b-jet backgrounds. An electromagnetic calorimeter isolation cut, centered on the axis of the 3 charged tracks, can be used to further suppress backgrounds with one or more  $\pi^0/\eta$ 's. A hadron calorimeter isolation cut on the excess hadron energy can be used to additionally suppress backgrounds with one or more  $K_L^0$  or neutrons present in the jet.

The mass resolution on the parent charmed particle,  $\sigma_M/M \simeq 0.7\%$  is extremely good for all-charged 3-body decay modes. This is illustrated in Fig. 4.13 for the decay  $D_s^+ \to K^+K^-\pi^+$ . Smearing the transverse momenta of the daughter kaons and the pion according to the CDF  $p_T$  resolution, a mass resolution of  $\sigma_{M_{D_s^+}} \simeq 13.5~{\rm MeV/c^2}$  is found. Cuts on a mass window, e.g.  $\pm 15~{\rm MeV/c^2}$  wide centered on  $M_{D^+}$ ,  $M_{D_s^+}$  can be made to further reduce backgrounds. It would be extremely useful to have the ability to distinguish  $\pi^\pm$  from  $K^\pm$  for these decays. However, the typical momenta of daughter particles from 3-body decays of charged charmed mesons from W decay is  $p_T \sim \frac{1}{3} \frac{M_W}{2} \sim 15~{\rm GeV/c}$ , which is very difficult to achieve for either dE/dX or time-of-flight measurements. Candidate events can be kept if an acceptable fit is found for either (or both) decay modes. The fraction of  $D^+$  vs.  $D_s^+$  can be determined via detailed MC simulations using kinematic information only, but can also be cross-checked via study of the proper decay-time distribution, since  $\tau_{D^+} \simeq 1.06~{\rm ps}$  and

# $D_s^+ \to K^+ K \ pi^+ from \ W^+ \to D_s^+ + \gamma \ Decays$

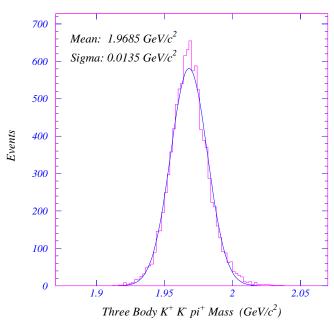


Figure 4.13: Invariant mass resolution for  $D_s^+ \to K^+ K^- \pi^+$  from  $W^+ \to D_s^+ \gamma$ .

 $\tau_{D_s^+} \simeq 0.47$  ps. Here again, we expect

$$\frac{BR(W^{\pm} \to D^{\pm}\gamma)}{BR(W^{\pm} \to D_{s}^{\pm}\gamma)} \simeq \frac{f_{D}^{2} |V_{cd}|^{2}}{f_{D_{s}}^{2} |V_{cs}|^{2}} \sim 0.034, \tag{4.27}$$

hence  $W^{\pm} \to D_s^{\pm} \gamma$  is expected to dominate. Experimentally, with a 10 fb<sup>-1</sup> data sample, 95% CL upper limits of  $BR(W^{\pm} \to D^{\pm} \gamma) < 10^{-5}$  and  $BR(W^{\pm} \to D_s^{\pm} \gamma) < 2 \times 10^{-5}$  could be achieved.

The decays  $W \to K^{\pm}\pi^0/K^0\pi^{\pm}$  are Cabbibo-suppressed relative to  $W \to \pi^{\pm}\pi^0$ . As we have mentioned above, the light quark background from the weak decay  $W \to q\bar{q}'$  has been estimated to be approximately two orders of magnitude higher than the  $W \to \pi\pi$  rate with current analysis techniques. It is not clear whether this two-body class of true rare W decays can ever be observed over this background. There is some optimism for improving the signal to background ratio. Whether or not it can be improved by two or more orders of magnitude remains to be demonstrated, and will certainly be a challenge! If it can, then with a 10 fb<sup>-1</sup> data sample, 95% CL upper limits of  $BR(W^{\pm} \to \pi^{\pm}\pi^{0}) < 10^{-7}$  and  $BR(W^{\pm} \to K^{\pm}\pi^{0}) < 2 \times 10^{-5}$  could be achieved.

Note however, that if the effective branching ratio  $BR(W \to q\bar{q}' \to \pi^{\pm} + "\gamma") \sim 3 \times 10^{-8}$  is actually this high, then this becomes an intriguing way in and of itself to potentially measure the W boson mass (and width) -i.e. force the jet fragmentation from  $W \to q\bar{q}'$  decays into the low charged track multiplicity region for both jets, use only the track momenta

and electromagnetic calorimeter information associated with the jet (which is well-measured) to compute  $M_{jj}$  on an event-by-event basis. The trigger used for capturing such events to tape is essentially a di-tau trigger.

There is somewhat greater hope for observing the rare decays  $W^+ \to D^0 K^+$  and  $W^+ \to D^+ K_L^0/K_S^0$ . The  $D^0$  meson has branching fractions to all-charged decay modes of  $BR(D^0 \to K^-\pi^+) \simeq 4.0\%$  and  $BR(D^0 \to K^-\pi^+\pi^+\pi^-) \simeq 8.1\%$ . Again, the dominant background here will be due to photon + charm and photon + B jet production. Event selection cuts very similar to those used for  $W^+ \to D^+(D_s^+)\gamma$  are equally useful here for  $D^0$  selection, in terms of rejecting/suppressing background. For the  $D^0K^+$  decay mode, a requirement of an isolated high  $p_T$  track is used for the  $K^+$ . Experimentally, with a 10 fb<sup>-1</sup> data sample, a 95% CL upper limit of  $BR(W^+ \to D^0K^+) < 6 \times 10^{-6}$  could be achieved.

For the  $W^+ \to D^+ K_L^0$  mode, the  $K_L^0$  is so long-lived that it is only detected via its shower, nearly entirely in the hadron calorimeter. Unfortunately, the resolution of typical hadron calorimeters is significantly worse than that for electromagnetic calorimeter. Hence the resolution on the W mass for this particular decay mode is  $\sigma_M/M \sim 12\%$ , requiring a larger W mass window of at least  $\pm 10~{\rm GeV/c^2}$  centered on  $M_W$ , which correspondingly lets in significantly more background. Experimentally, with a  $10^{-1}$  fb data sample, a 95% CL upper limit of  $BR(W^+ \to D^+ K_L^0) < 8 \times 10^{-5}$  could be achieved.

For the  $W^+ \to D^+ K^0_S$  mode, the  $K^0_S$  decays  $\sim 69\%$  of the time to  $\pi^+\pi^-$ . The typical decay length for a  $K^0_S$  from  $W^+ \to D^+ K^0_S$  decay is  $L_{K^0_S} = \gamma \beta c \tau \simeq 215$  cm. Hence the  $K^0_S \to \pi^+\pi^-$  and overall  $W^+ \to D^+ K^0_S$  reconstruction efficiency will be exceedingly small, due to the relatively long lifetime of the  $K^0_S$  meson.

In summary, the experimental sensitivities for rare W decays and 10 fb<sup>-1</sup> are expected to be at least two orders of magnitude away from the branching ratios estimated in the SM. However, since the SM estimates are quite uncertain, a continued and extended search for  $W \to P\gamma$  and  $W \to P_1P_2$  decays will yield useful information on our understanding of decay form factors in the high momentum transfer regime.

# 4.6 Searching for CP Violation in W Production and Decay

#### 4.6.1 Preliminaries

The origin of CP violation remains one of the unsolved questions in particle physics. It is therefore imperative to search for signals of CP violation in all experimentally accessible processes. The Tevatron offers a unique opportunity to search for CP violation in W boson production and decay because it collides protons and antiprotons, *i.e.* the initial state is a CP eigenstate. The extremely large number of W boson events expected at a superluminous Tevatron will make it possible to look for small CP violating contributions to W boson production. CP violating effects can affect W production in various different ways. CP nonconservation in parton distribution functions, or at higher twist, is one possibility. In this case one would expect that other processes such as inclusive jet production also possess a CP violating component. Here we shall concentrate on CP violation in the Wqq' and

 $W\ell\nu$  vertices. Our discussion closely follows that of Ref. [4], which complements Refs. [50] and [51].

Kaon, charm and B-decay decay experiments tell us that CP violating effects in the SM are extremely small. In addition, CP odd observables in the SM vanish in the limit of massless fermions. The SM does not produce a sufficiently large CP odd signal to be observed with the number of W boson events anticipated at the Tevatron with 10 fb<sup>-1</sup> [52]. Popular extensions of the SM in the context of CP violation include multi-Higgs boson models. In these models, CP violation is also proportional to fermion masses and thus negligible in the processes we are interested in. We shall, therefore, assume that studies of CP violation in W production at hadron colliders will only be sensitive to non-SM sources. To parameterize possible CP violating operators, we shall use an effective Lagrangian approach. The operators are assumed to originate from the mechanism which breaks the electroweak symmetry.

### **4.6.2** $p\bar{p} \to W^{\pm}X \to \ell^{\pm}\nu X$

Under a CP transformation, the lepton rapidities and transverse momenta transform as

$$y_{\ell^-} \stackrel{CP}{\longleftrightarrow} -y_{\ell^+}, \quad p_{T\ell^-} \stackrel{CP}{\longleftrightarrow} p_{T\ell^+}.$$
 (4.28)

In terms of these variables the simplest CP-odd observables which can be constructed are the asymmetries:

$$\tilde{R}_{1} \equiv \frac{\sigma^{+} - \sigma^{-}}{\sigma^{+} + \sigma^{-}}$$

$$\tilde{R}_{2}(y_{0}) \equiv \frac{\frac{d\sigma^{+}}{dy_{\ell}} \left| y_{\ell} = y_{0} - \frac{d\sigma^{-}}{dy_{\ell}} \right| y_{\ell} = -y_{0}}{\frac{d\sigma^{+}}{dy_{\ell}} \left| y_{\ell} = y_{0} + \frac{d\sigma^{-}}{dy_{\ell}} \right| y_{\ell} = -y_{0}}$$

$$\tilde{R}_{3}(p_{T}) \equiv \frac{\frac{d\sigma^{+}}{dp_{T}} - \frac{d\sigma^{-}}{dp_{T}}}{\frac{d\sigma^{+}}{dp_{T}} + \frac{d\sigma^{-}}{dp_{T}}}, \tag{4.29}$$

where  $\sigma^{\pm}$  refers to  $\sigma(p\bar{p} \to \ell^{\pm}\nu X)$ .

If the p and  $\bar{p}$  beams are unpolarized, and the polarization of the final state lepton is not measured, it is necessary to have an absorptive phase,  $\phi$ , in order to generate the CP odd observables in Eq. (4.29). In the following we consider the CP violating four-fermion operator

$$\mathcal{L}_{CP} = \frac{4\pi}{\Lambda^2} e^{i\phi} \overline{c}_L \gamma_\mu s_L \overline{\ell}_L \gamma^\mu \nu_L + \text{ h. c.}$$
 (4.30)

where  $\Lambda$  is the scale of new physics. We consider the operator Eq. (4.30), instead of a similar one with  $\bar{u}d$  quarks for two reasons. First, for the operator with  $\bar{u}d$  there is a cancellation between two contributions to  $p\bar{p} \to \ell^{\pm}\nu$  as discussed in Ref. [50]. This cancellation is exact for the resonant process studied here, but it does not occur for the operator with  $\bar{c}s$  of Eq. (4.30). Furthermore, while there are several indirect constraints from low energy experiments on the operator with  $\bar{u}d$  [50], analogous constraints on the operator in Eq. (4.30) depend on naturalness assumptions.

In the narrow W width approximation, the operator of Eq. (4.30) results in

$$\tilde{R}_1 = \tilde{R}_2(y_0) = \tilde{R}_3(p_T) \approx -\frac{1}{3} \frac{M_W^2}{\Lambda^2} \sin \phi$$
 (4.31)

for the CP violating asymmetries. In order to observe a signal at the one-standard deviation level, the number of W boson events, N, for integrated asymmetries is required to be greater than

$$N > \frac{1}{\tilde{R}_1^2} \approx 200,000 \left(\frac{\Lambda}{1 \text{ TeV}}\right)^4 \frac{1}{\sin^2 \phi} .$$
 (4.32)

For the W event sample expected at the Tevatron for 10 fb<sup>-1</sup>, it should in principle be possible to observe CP violation coming from new physics at the TeV scale.

**4.6.3** 
$$p\bar{p} \to W^{\pm} + 1 \text{ jet} \to \ell^{\pm}\nu + 1 \text{ jet}$$

In this process there are several parton subprocesses that contribute at leading order in  $\alpha_s$  and there are enough independent four-vectors to give rise to T-odd correlations. The interest of these correlations lies in the fact that they can generate CP odd observables without requiring additional absorptive phases and thus may test different types of CP violating physics than the asymmetries of Eq. (4.29).

For the W+1 jet process there is one T-odd correlation that can be observed; in the laboratory frame it is given by the triple product  $\vec{p}_{\ell} \cdot (\vec{p}_{\text{beam}} \times \vec{p}_{\text{jet}})$ . There are several equivalent ways to use this correlation to construct a T-odd observable. The basic idea is to define the plane formed by the beam and jet momenta and count the number of events with the lepton above the plane minus the number of events with the lepton below the plane:

$$A^{\pm} = \sigma^{\pm} [(\vec{p}_{\text{beam}} \times \vec{p}_{\text{jet}}) \cdot \vec{p}_{\ell} > 0] - \sigma^{\pm} [(\vec{p}_{\text{beam}} \times \vec{p}_{\text{jet}}) \cdot \vec{p}_{\ell} < 0]. \tag{4.33}$$

Here,  $A^{\pm}$  refers to the observable for  $W^{\pm}$  events (or  $\ell^{\pm}\nu$  events). A practical way to implement this observable in the calculation (or in the experiment) is to weigh the matrix element squared for a parton subprocess (or to weigh the observed event) by the sign of  $\vec{p}_{\ell} \cdot (\vec{p}_{\text{beam}} \times \vec{p}_{\text{jet}})$ . Invariance under a CP transformation predicts that  $A^{+} = A^{-}$ .

To use jet variables it is necessary to assume that the algorithm that defines the jet is CP blind in the sense that the probability of finding that a collection of particles with certain momenta forms a jet is the same as the probability of finding that a collection of the respective anti-particles with the momenta reversed forms a jet. No simulations have been carried out so far to verify this assumption.

Analogous to the observables of Eq. (4.29), it is useful to construct not only the fully integrated asymmetry, but asymmetries for distributions as well. One obvious reason is that the simultaneous study of the different distribution asymmetries provides a handle on the possible CP odd biases of a detector. Another reason is that it is possible for the integrated asymmetry to vanish while having non-vanishing asymmetries for distributions. Some T-odd CP odd observables are then:

$$R_1 \equiv \frac{A^+ - A^-}{\sigma^+ + \sigma^-}$$

$$R_{2}(y_{0}) \equiv \frac{\frac{dA^{+}}{dy} |_{y=y_{0}} - \frac{dA^{-}}{dy} |_{y=-y_{0}}}{\frac{d\sigma^{+}}{dy} |_{y=y_{0}} + \frac{d\sigma^{-}}{dy} |_{y=-y_{0}}}$$

$$R_{3}(p_{T}) \equiv \frac{\frac{dA^{+}}{dp_{T}} - \frac{dA^{-}}{dp_{T}}}{\frac{d\sigma^{+}}{dp_{T}} + \frac{d\sigma^{-}}{dp_{T}}},$$
(4.34)

where y and  $p_T$  represent the rapidity and transverse momentum of the lepton or the jet (or the W).

CP violating triple product correlations of the form (4.33) require operators which depend on the momentum carried by the fermions in the  $Wf\overline{f'}$  coupling such as

$$\mathcal{L} = -\frac{\sqrt{2}}{\Lambda^2} \left[ \tilde{\kappa} \overline{\Psi}_L \overleftarrow{D}_{\alpha} \gamma_{\mu} \Sigma \tau_{-} \Sigma^{\dagger} \overrightarrow{D}^{\alpha} \Psi_L \Sigma_{+}^{\mu} + \tilde{\kappa}^{\star} \overline{\Psi}_L \overleftarrow{D}_{\alpha} \gamma_{\mu} \Sigma \tau_{+} \Sigma^{\dagger} \overrightarrow{D}^{\alpha} \Psi_L \Sigma_{-}^{\mu} \right]. \tag{4.35}$$

In unitary gauge  $\Sigma = 1$  and  $\Sigma_{\pm}^{\mu} = -\frac{g}{2}W^{\mu\pm}$ . For the processes of interest there is only one W boson and no Z bosons, so the covariant derivatives refer only to QED and QCD:

$$D_{\alpha}\Psi_{L} \to \left(\partial_{\alpha} + \frac{i}{2}g_{S}\lambda^{a}G_{\alpha}^{a} + ieQA_{\alpha}\right)\left(\begin{array}{c} u\\ d_{\theta} \end{array}\right)_{L}.$$
(4.36)

The fully integrated asymmetry  $R_1$  vanishes for the interaction of Eq. (4.35). The asymmetry in the electron rapidity distribution,  $R_2(y_e)$ , is shown in Fig. 4.14 for  $Im \ \tilde{\kappa} = 1$  and  $\Lambda = 1$  TeV. A transverse momentum cut of  $p_{Tjet} > 30$  GeV, and a rapidity cut of  $|y_{jet}| < 3$  are imposed on the jet. At the one standard deviation level some  $10^6 \ W^{\pm}$  plus one jet events are needed to observe this asymmetry. For 10 fb<sup>-1</sup> one expects approximately  $0.5 \cdot 10^6 \ W + 1$  jet events within the cuts listed above. Lowering the  $p_{Tjet}$  cut to, say, 15 GeV would result in a larger event sample.  $R_2(y_e)$  depends only marginally on the jet transverse momentum threshold. If the background can be controlled at the level required (see Section 6.4) to observe CP-violating effects for the lower  $p_T$  threshold, it should be possible to observe  $R_2(y_e)$  for the values of  $\tilde{\kappa}$  and  $\Lambda$  chosen. It should be noted, however, that measuring this asymmetry for arbitrary values of  $y_e$  is complicated by the fact that the acceptance of the detector must be the same for  $y_e$  and  $y_e$ . Figure 4.14 shows that the asymmetry does not necessarily vanish at  $y_e = 0$ , making this a particularly interesting point to search for CP violation.

### 4.6.4 Detector Requirements

In order to be sensitive to CP-violating effects at the  $10^{-3}$  level and below in W boson production and decay, it is necessary to have a detector that is intrinsically "CP-symmetric" to better than the anticipated sensitivity level of CP violation, as was the case for each of the "classic" fixed target experiments that first discovered, and then measured CP violation in the neutral K-meson system.

For example, for a sample of  $W \to e\nu$  events associated with an integrated luminosity of 10 (100) fb<sup>-1</sup>, obtained with standard CDF/DØ lepton trigger and identification cuts, the statistical accuracy for integrated asymmetries is approximately  $4 \times 10^{-4}$  (1.25 × 10<sup>-4</sup>). For

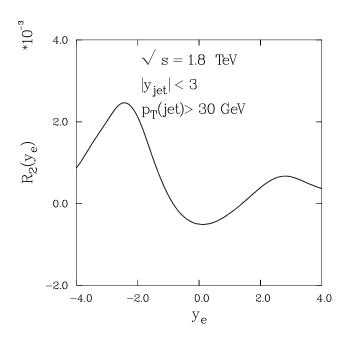


Figure 4.14: CP violating asymmetry in the lepton rapidity distributions as defined in Eq. (4.34) for  $\Lambda = 1$  TeV and  $Im \ \tilde{\kappa} = 1$ .  $R_2(y_e)$  scales as  $Im \ \tilde{\kappa}/\Lambda^2$ .

differential asymmetries, such as lepton rapidity binned in units of  $\Delta y_e = 0.2$  the statistical accuracy per bin is  $\sim 1.25 \times 10^{-3}~(4 \times 10^{-4})$ . A similar analysis for W+1 jet events yields a statistical accuracy per bin of  $\sim 5 \times 10^{-3}~(1.6 \times 10^{-3})$  for  $p_{Tjet} > 30$  GeV and  $|y_{jet}| < 3$ . This is shown in Fig. 4.15 for  $\tilde{R}_2(y_e)$  in inclusive  $W \to e\nu$  production with 10 fb<sup>-1</sup>, and  $R_2(y_e)$  for W+1 jet,  $W \to e\nu$ , production with the  $p_T$  and rapidity cuts listed above. For  $\tilde{R}_2(y_e)$  we also display the value expected from Eq. (4.31) for  $\Lambda=1$  TeV and  $\sin\phi=1$  (dashed horizontal line). Thus, all contributions from systematic effects — detector biases at the trigger level and offline analysis must be less than the above statistical uncertainties for integral and/or differential asymmetries.

There are numerous potential sources of detector bias which can in principle mimic a false CP-violating effect. Fortunately, most, if not all of these can be adequately dealt with in such types of analyses. While in principle the response of an electromagnetic calorimeter is identical to high  $p_T$  electrons and positrons at the trigger level and in offline analysis, dead, noisy or mis-calibrated calorimeter towers can introduce a CP-bias due to the intrinsic charge asymmetry in W production and decay. However, such effects are routinely monitored during data-taking, and can be properly taken into account. The relative response of the electromagnetic calorimeter is calibrated using high-statistics samples of inclusive electrons taken throughout the run. The absolute energy scale can be determined e.q. by fitting the lineshape of the E/p distribution from  $W \to e\nu$  decay, cross-checking the E/p distribution for inclusive electrons versus positrons and  $W^+$  versus  $W^-$  decays as a function of  $y_e$ ,  $E_T^e$  $p_T^e$  and  $M_T^W$ , as well as e.g. studies of the E/p distribution for  $e^+$  versus  $e^-$  from  $Z \to e^+e^$ production and decay. The absolute energy scale of the electromagnetic calorimeter can also be independently cross-checked using  $Z \to e^+e^-$  data. Time-dependent effects on electromagnetic calorimeter gain calibrations can in principle be adequately accounted for via these methods.

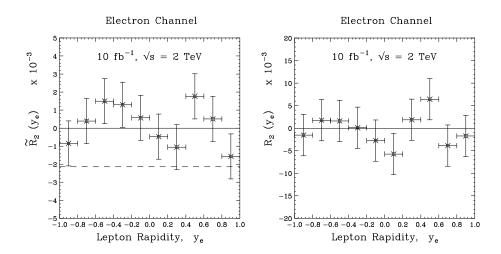


Figure 4.15: Statistical accuracy for 10 fb<sup>-1</sup> of  $\tilde{R}_2(y_e)$  for inclusive  $W \to e\nu$  production, and  $R_2(y_e)$  for W+1 jet,  $W \to e\nu$ , production with the  $p_T$  and rapidity cuts listed in the text, versus  $y_e$ . Also shown is what one expects for  $\tilde{R}_2(y_e)$  from Eq. (4.31) for  $\Lambda=1$  TeV and  $\sin \phi = 1$  (dashed horizontal line).

If the event vertex is not located at the symmetry point of the detector (z=0), but is shifted away from this point, a CP-bias can arise. Again, the event vertex distribution is routinely monitored throughout the data-taking run and can be explicitly corrected for in the offline analysis. In principle, the best way to control this potential systematic effect is to ensure that the data being taken is properly located in z throughout the entire run.

The missing transverse energy,  $E_T$ , is calculated using the transverse energy of the electron as measured in the calorimeter and the transverse energy deposited in the calorimeter by the rest of the event excluding the electron, U. Assuming there is no manifest CP-bias associated with the  $E_T^e$  distribution, it is still possible to induce a false CP-effect if it originates with U. The transverse energy U associated with the underlying event is measured in the calorimeter, and is typically such that  $U \ll E_T^e$ . A CP-bias can arise in U e.g, from mis-calibration effects at low  $E_T$  in the two detector hemispheres, which can asymmetrically couple into  $W^+$  versus  $W^-$  production due to the intrinsic charge asymmetry associated with W production and decay. Fortunately, it is again possible to monitor (and compensate) for such biases in U throughout the data-taking by using high-statistics samples of minimum bias data, and ensuring that the low  $E_T$  response of both the electromagnetic and hadron calorimeter towers of the detector are CP-symmetric to the required degree of accuracy. Note also that U is measured using all, or nearly all of the calorimeter rapidity coverage of the detector.

A false CP-violating U can potentially also be induced from higher-order QCD effects [53] associated with W+ jet production, due to a few-percent asymmetry in the jet angular distribution and mis-calibration of the calorimeters in the two detector hemispheres. Again, this potential bias can in principle be properly and fully accounted for, in a careful analysis.

For CP violation studies involving triple-product type tests using W+ jet data samples, e.g. for  $p_{Tjet} > 30$  GeV, gain and efficiency variations across the hadronic calorimeter at this energy scale must also be known throughout the run, in addition to those for the electromagnetic calorimeter. High-statistics samples of minimum bias data, di-jet and/or photon+jet data can be used for accomplishing this task if one assumes that the data sample(s) used for such calibration(s) do not contain a manifestly CP-violating process, at least a comparable level to that being searched for in the primary  $W \to e\nu$  data sample.

An important and useful cross check on any observed CP-violating signal in the electron W data sample can be obtained by repeating the analysis using muon W data. The systematics associated with these two W decay channels are not identical. Electrons from W decay can be, and currently are, obtained using a calorimeter-only based trigger. They can be obtained as well as from an independent calorimeter + tracking trigger. Muons from W decay are obtained primarily using a tracking trigger. The  $E_T$  is calculated using the transverse energy of the electron or muon track  $p_T^\mu$  and the transverse energy associated with the underlying event, U. Verifying that the tracking devices in the experiment do not introduce a false CP-violating signal at the trigger and/or offline level also requires some degree of effort. Assuming no such effects to be present in  $J/\psi$ ,  $\Upsilon$  and  $Z \to \ell^+\ell^-$  production and decay, these data samples, acquired simultaneously throughout the run can be used to search for, and place limits on tracking induced CP-biases. Since the number of Z boson events is approximately one order of magnitude smaller than the number of W candidates, the Z sample alone will not be able to place constraints on potential CP-biases at the level required for the W data.

Assuming that the results associated with the muon channel W data sample are compatible with those from the electron W data sample and that lepton universality holds in such CP violation searches, combining muon W data with electron W data results in an improvement by a factor of  $\sqrt{2}$  in statistical sensitivity of the physics result.

Similarly, it is worthwhile to carry out searches for CP violation in W production and decay using tau W data samples. Even though tau W data samples historically have reduced statistical power, due to the reduction in  $W \to \tau \nu$  trigger efficiency and offline analysis cuts relative to electron/muon W data, they still have sufficient statistical power, and quite different systematics to warrant studying them for such effects.

# 4.7 Di-boson Production and Anomalous Gauge Boson Couplings

#### 4.7.1 Introduction

One of the most direct consequences of the  $SU(2)_L \times U(1)_Y$  gauge symmetry are the non-abelian self-couplings of the W, Z and photon  $(WWV, Z\gamma V, V = \gamma, Z, WW\gamma\gamma)$  etc.). A direct measurement of the three vector boson couplings at the Tevatron is possible through the study of pair production processes like  $q\bar{q} \to W^+W^-, W\gamma, Z\gamma, WZ$ . Quartic couplings can be probed in multi weak boson production, such as  $p\bar{p} \to W\gamma\gamma, WWZ$ , etc. Here we shall concentrate on the measurement of the three gauge boson couplings.

Analogous to the introduction of arbitrary vector and axial vector couplings  $g_V$  and  $g_A$  for the coupling of gauge bosons to fermions, the measurement of the WWV couplings can be made quantitative by introducing a more general WWV vertex. For our discussion of experimental sensitivities below we shall use a parameterization in terms of the phenomenological effective Lagrangian [54]

$$i\mathcal{L}_{eff}^{WWV} = g_{WWV} \left[ g_1^V \left( W_{\mu\nu}^{\dagger} W^{\mu} - W^{\dagger\mu} W_{\mu\nu} \right) V^{\nu} + \kappa_V W_{\mu}^{\dagger} W_{\nu} V^{\mu\nu} + \frac{\lambda_V}{M_W^2} W_{\rho\mu}^{\dagger} W^{\mu}_{\nu} V^{\nu\rho} + i g_5^V \varepsilon_{\mu\nu\rho\sigma} \left( (\partial^{\rho} W^{\dagger\mu}) W^{\nu} - W^{\dagger\mu} (\partial^{\rho} W^{\nu}) \right) V^{\sigma} \right].$$

$$(4.37)$$

Here the overall couplings are defined as  $g_{WW\gamma} = e$  and  $g_{WWZ} = e \cot \theta_W$ ,  $W_{\mu\nu} = \partial_{\mu}W_{\nu} - \partial_{\nu}W_{\mu}$ , and  $V_{\mu\nu} = \partial_{\mu}V_{\nu} - \partial_{\nu}V_{\mu}$ . Within the SM, at tree level, the couplings are given by  $g_1^Z = g_1^{\gamma} = \kappa_Z = \kappa_{\gamma} = 1$ ,  $\lambda_Z = \lambda_{\gamma} = g_5^Z = g_5^{\gamma} = 0$ . For on-shell photons,  $g_1^{\gamma} = 1$  and  $g_5^{\gamma} = 0$  are fixed by electromagnetic gauge invariance;  $g_1^Z$  and  $g_5^Z$  may, however, differ from their SM values. Deviations are given by the anomalous coupling parameters

$$\Delta g_1^Z \equiv (g_1^Z - 1) , \quad \Delta \kappa_\gamma \equiv (\kappa_\gamma - 1) , \quad \Delta \kappa_Z \equiv (\kappa_Z - 1) , \quad \lambda_\gamma , \quad \lambda_Z , \quad g_5^Z .$$
 (4.38)

To simplify our discussion, we shall assume  $g_5^Z=0$  in the following. The effective Lagrangian of Eq. (4.37) parameterizes the most general Lorentz invariant and CP conserving WWV vertex which can be observed in processes where the vector bosons couple to effectively massless fermions. The C and P conserving terms in  $\mathcal{L}_{eff}^{WW\gamma}$  correspond to the lowest order terms in a multipole expansion of the W-photon interactions, the charge  $Q_W$ , the magnetic dipole moment  $\mu_W$  and the electric quadrupole moment  $q_W$  of the  $W^+$  [55]:

$$Q_W = eg_1^{\gamma} , \qquad (4.39)$$

$$\mu_W = \frac{e}{2M_W} \left( g_1^{\gamma} + \kappa_{\gamma} + \lambda_{\gamma} \right) , \qquad (4.40)$$

$$q_W = -\frac{e}{M_W^2} \left(\kappa_\gamma - \lambda_\gamma\right) . \tag{4.41}$$

Analogous to the general WWV vertex it is possible to parameterize anomalous  $Z\gamma V, V = \gamma, Z$  couplings. In the following, we shall be interested in constraints from  $Z\gamma$  production processes, *i.e.* we may treat the photon and the Z as being on-shell. As before we are only considering CP-even couplings. Let us denote the Feynman rule for the  $V_{\mu}(P) \to Z_{\alpha}(q_1)\gamma_{\beta}(q_2)$  vertex by  $ie\Gamma_{Z\gamma V}^{\alpha\beta\mu}(q_1,q_2,P)$ . The most general such vertex compatible with Lorentz invariance has been discussed in Ref. [54] and it can be parameterized in terms of two free parameters,  $h_3^V$  and  $h_4^V$ ,

$$\Gamma_{Z\gamma V}^{\alpha\beta\mu}(q_1, q_2, P) = \frac{P^2 - M_V^2}{M_Z^2} \left[ h_3^V \varepsilon^{\mu\alpha\beta\rho} q_{2\rho} + \frac{h_4^V}{M_Z^2} P^\alpha \varepsilon^{\mu\beta\rho\sigma} P_\rho q_{2\sigma} \right]. \tag{4.42}$$

Within the SM, at tree level,  $h_3^V = h_4^V = 0$ . The overall factor  $P^2 - m_V^2$  in Eq. (4.42) is implied by Bose symmetry for on-shell V and/or by gauge invariance for  $V = \gamma$ .

Because of the subtle cancellations between the different processes for di-boson production in the Standard Model, any deviation of the couplings from their standard model

values will result in an increase in cross section. While the SM contributions to the di-boson production amplitudes are bounded from above for fixed scattering angles, the anomalous contributions rise without limit as the parton center of mass energy squared,  $\hat{s}$ , increases, eventually violating S-matrix unitarity. Anomalous couplings therefore must show a form factor behaviour at very high energies [56]. In our subsequent analysis we will assume a simple power law behaviour, e.g.

$$\Delta \kappa_V(\hat{s}) = \frac{\Delta \kappa_V^0}{(1 + \hat{s}/\Lambda_{FF}^2)^n} , \qquad (4.43)$$

and similarly for the other couplings. Here,  $\Lambda_{FF}$  is the form factor scale which is a function of the scale of new physics,  $\Lambda$ , which is responsible for the non-standard vector boson self-interactions. For WWV couplings we shall use the exponent n=2, which will be referred to as the 'dipole form factor' below. For  $Z\gamma V$  couplings we choose n=3 (n=4) for  $h_3^V$  ( $h_4^V$ ). Due to the form factor behaviour of the anomalous couplings, the experimental limits extracted from hadron collider experiments explicitly depend on  $\Lambda_{FF}$ .

Information on anomalous WWV and  $Z\gamma V$  couplings can be obtained by comparing the shape of measured and predicted distributions which reflect the high energy behaviour of the di-boson production amplitudes, such as the  $p_T$  distribution of the W, Z or photon.

#### 4.7.2 Present Tevatron Limits

The CDF and DØ Collaborations have observed  $W\gamma$  [57, 58, 59],  $Z\gamma$  [59, 60, 61],  $W^+W^-$  [62, 63, 64], and WZ [62, 64] production in the data samples accumulated in Run 1a and 1b. Di-boson data samples are extracted from inclusive  $e/\mu$  channel W/Z data. The main background for  $W\gamma$  and  $Z\gamma$  production is W/Z+ jet(s) production, where one of the jets fakes an isolated photon. In its  $WW,WZ\to\ell\nu jj$  and  $ZW\to\ell^+\ell^- jj$  analysis, CDF eliminates the W/Z+ jets background by requiring 60 GeV/c<sup>2</sup> < m(jj) < 110 GeV/c<sup>2</sup> and  $p_T(jj) > 130$  (100) GeV/c [62]. This also eliminates the SM signal but retains good sensitivity for non-zero WWV anomalous couplings. DØ, in its  $WW,WZ\to e\nu jj$  analysis, performs a fit to the  $p_T(jj)$  distribution for  $W+\geq 2$  jet,  $W\to e\nu$ , events with 50 GeV/c<sup>2</sup> < m(jj) < 110 GeV/c<sup>2</sup> [64]. The muon channel is not considered. In the  $WW\to\ell_1\nu_1\ell_2\nu_2$ ,  $\ell_{1,2}=e,\mu$ , channels,  $\bar{t}t$  production constitutes the most significant background. It can be removed either through a jet veto, or a cut on the transverse energy of the hadrons in the event [63].

Direct experimental limits on  $WW\gamma$  and  $Z\gamma V$  anomalous couplings for the  $W\gamma/Z\gamma$  processes are obtained via binned maximum likelihood fits to the  $E_T(\gamma)$  distribution. Bounds from the  $\ell\nu jj$  and  $\ell^+\ell^-jj$  final states are extracted via comparison of observed events to the expected signal within cuts, including systematic uncertainties due to luminosity normalization, jet energy scale and resolution, structure function choice and higher order QCD corrections, etc. Limits on WWV anomalous couplings from the  $WW \to \ell_1 \nu_1 \ell_2 \nu_2$  mode have been derived via comparison of the 95% CL upper limit of  $\sigma(WW)_{expt} < 87$  pb (DØ) with  $\sigma(WW)_{pred}$  as a function of the anomalous couplings.

The limits obtained from  $W^+W^- \to \ell_1\nu_1\ell_2\nu_2$  and  $WW, WZ \to \ell\nu jj$  are summarized and compared to those obtained from  $W\gamma$  production in Fig. 4.16a. In extracting limits on

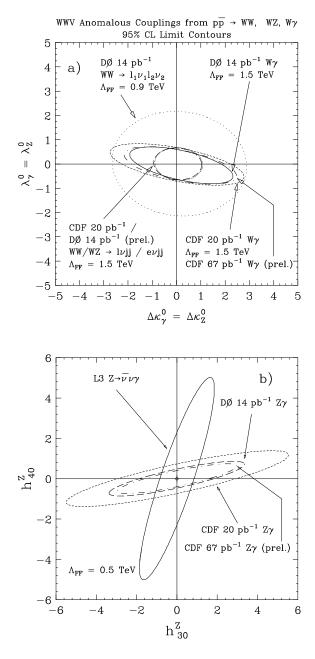


Figure 4.16: Present limits on anomalous WWV and  $ZZ\gamma$  couplings from Tevatron and LEP experiments.

non-standard WWV couplings from W pair production,  $\Delta \kappa_{\gamma}^{0} = \Delta \kappa_{Z}^{0}$ ,  $\lambda_{\gamma}^{0} = \lambda_{Z}^{0}$ , and  $\Delta g_{1}^{Z} = 0$  have been assumed. The 95% CL limit contours from the current CDF WW,  $WZ \rightarrow \ell \nu jj$  and DØ WW,  $WZ \rightarrow \epsilon \nu jj$  searches are almost identical.

The current CDF [60] and DØ [61] 95% CL limit contours for anomalous  $ZZ\gamma$  couplings are shown in Fig. 4.16b, together with the L3 constraint from  $e^+e^- \to \bar{\nu}\nu\gamma$  [65]. In order to derive these limits, generalized dipole form factors with  $\Lambda_{FF}=0.5$  TeV, and powers n=3 (n=4) for  $h_3^V$  ( $h_4^V$ ), are assumed. LEP and Tevatron experiments are seen to yield complementary information on  $ZZ\gamma$  couplings. Since the anomalous contributions to the  $Z\gamma$  helicity amplitudes grow faster with energy than those in  $W\gamma$  production, the experimental limits on  $h_{30}^V$  and  $h_{40}^V$  depend rather sensitively on the form factor scale chosen. The maximum form factor scale which can be probed with present experimental data is  $\Lambda_{FF}\approx 500$  GeV; for larger values S-matrix unitarity yields stronger bounds. The limit contours for  $Z\gamma\gamma$  couplings obtained by CDF and DØ are similar to those shown in Fig. 4.16b for  $ZZ\gamma$  couplings. Single photon production at LEP is very insensitive to  $Z\gamma\gamma$  couplings.

Table 4.5 summarizes the current results on anomalous WWV and  $Z\gamma V$  couplings from colliders. With the limited statistics of di-boson events currently available, deviations from the SM cross section have to be large at least in some regions of phase space in order to lead to an observable effect. The best direct limits on  $\Delta \kappa_V^0$  are currently obtained from the  $\ell \nu jj$  final state.  $W\gamma$  production results in somewhat better bounds on  $\lambda_\gamma^0$  than  $p\bar{p} \to WW, WZ \to \ell \nu jj$ . So far, no attempt has been made to combine the limits of CDF and DØ and/or from different channels.

#### 4.7.3 Expectations for the Main Injector Era and Beyond

The substantial increase in integrated luminosity expected in the future will make it possible to test the WWV and  $Z\gamma V$  vertices at the Tevatron with much greater precision than in current experiments. In Figs. 4.17 and 4.18 we show the 95% CL limits on anomalous  $WW\gamma$  and  $ZZ\gamma$  couplings expected from  $W\gamma$  and  $Z\gamma$  production at the Tevatron for high integrated luminosities. Here, and in all subsequent sensitivity plots, we assume that no deviation from the SM prediction is observed in future experiments. To derive bounds on non-standard WWV couplings, a dipole form factor is assumed. For the  $Z\gamma V$  couplings we use form factor powers of n=3  $(h_3^V)$  and n=4  $(h_4^V)$ . The limits on  $Z\gamma\gamma$  couplings are very similar to those found for  $ZZ\gamma$  couplings and are therefore not shown.

For  $W\gamma$  production, the  $W\to e\nu$  channel is analyzed. The electron is required to have  $|\eta(e)|<1.0$ , and a pseudorapidity cut of  $|\eta(\gamma)|<2.4$  is imposed on the photon. The acceptances are calculated using the following transverse energy and separation cuts:

$$E_T(e) > 25 \text{ GeV}, \qquad E_T > 25 \text{ GeV}, \qquad (4.44)$$

$$E_T(\gamma) > 10 \text{ GeV}, \qquad \Delta R(e, \gamma) > 0.7.$$
 (4.45)

In addition, a cut on the transverse W mass of  $m_T^W > 50 \text{ GeV/c}^2$  and a cluster transverse mass cut of  $m_T(e\gamma; E_T) > 90 \text{ GeV/c}^2$  are imposed. The efficiencies for electron and photon identification were taken from the current CDF analysis, as well as the probability for a jet to fake a photon,  $\mathcal{P}_{j\to\gamma}(E_T)$ . The systematic uncertainty from the integrated luminosity,

Table 4.5: 95% CL limits on anomalous WWV,  $V=\gamma$ , Z, and  $ZZ\gamma$  couplings from collider experiments. Only one of the independent couplings is allowed to deviate from the SM at a time. The bounds obtained by CDF and DØ for  $Z\gamma\gamma$  couplings are very similar to those derived for the  $ZZ\gamma$  couplings and are therefore not shown.

experiment	channel	limit
CDF (prel.) 67 pb <sup>-1</sup>	$p\bar{p} \to W^{\pm}\gamma \to \ell^{\pm}\nu\gamma$ $\ell = e, \mu$	$-1.8 < \Delta \kappa_{\gamma}^{0} < 2.0$ $-0.7 < \lambda_{\gamma}^{0} < 0.6$
DØ 14 pb <sup>-1</sup>	$p\bar{p} \to W^{\pm}\gamma \to \ell^{\pm}\nu\gamma$ $\ell = e, \mu$	$-1.6 < \Delta \kappa_{\gamma}^{0} < 1.8$ $-0.6 < \lambda_{\gamma}^{0} < 0.6$
$CDF$ $20 \text{ pb}^{-1}$	$p\bar{p} \to W^{\pm}Z \to \ell^{+}\ell^{-}jj$ $\ell = e, \mu$	$-8.6 < \Delta \kappa_Z^0 < 9.0$ $-1.7 < \lambda_Z^0 < 1.7$
$CDF$ $20 \text{ pb}^{-1}$	$p\bar{p} \to W^+W^-, W^{\pm}Z \to \ell^{\pm}\nu jj$ $\ell = e, \mu, \kappa_{\gamma} = \kappa_Z, \lambda_{\gamma} = \lambda_Z$	$-1.0 < \Delta \kappa_V^0 < 1.0  -0.6 < \lambda_V^0 < 0.7$
DØ (prel.) 14 pb <sup>-1</sup>	$p\bar{p} \to W^+W^-, W^{\pm}Z \to e^{\pm}\nu jj$ $\kappa_{\gamma} = \kappa_Z, \ \lambda_{\gamma} = \lambda_Z$	$-0.9 < \Delta \kappa_V^0 < 1.1  -0.7 < \lambda_V^0 < 0.7$
DØ 14 pb <sup>-1</sup>	$p\bar{p} \to W^+W^- \to \ell_1\nu_1\ell_2\nu_2$ $\ell_{1,2} = e,  \mu,  \kappa_{\gamma} = \kappa_Z,  \lambda_{\gamma} = \lambda_Z$	$-2.6 < \Delta \kappa_V^0 < 2.8$ $-2.2 < \lambda_V^0 < 2.2$
CDF (prel.) 67 pb <sup>-1</sup>	$p\bar{p} \to Z\gamma \to \ell^+\ell^-\gamma$ $\ell = e,  \mu,  \Lambda_{FF} = 0.5 \text{ TeV}$	$-1.6 < h_{30}^Z < 1.6$ $-0.4 < h_{40}^Z < 0.4$
DØ 14 pb <sup>-1</sup>	$p\bar{p} \to Z\gamma \to \ell^+\ell^-\gamma$ $\ell = e,  \mu,  \Lambda_{FF} = 0.5 \text{ TeV}$	$-1.9 < h_{30}^Z < 1.8$ $-0.5 < h_{40}^Z < 0.5$
L3	$e^+e^- \to Z \to \bar{\nu}\nu\gamma$ $\Lambda_{FF} = 0.5 \text{ TeV}$	$-0.85 < h_{30}^Z < 0.85$ $-2.32 < h_{40}^Z < 2.32$

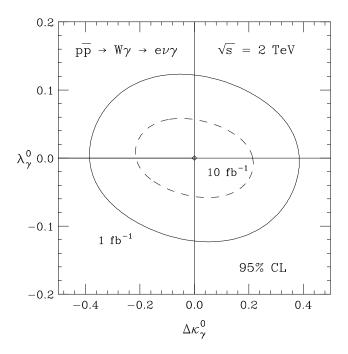


Figure 4.17: Projected 95% CL sensitivity limits for  $WW\gamma$  couplings from  $W\gamma$  production at the Tevatron for integrated luminosities of 1 fb<sup>-1</sup> and 10 fb<sup>-1</sup>.

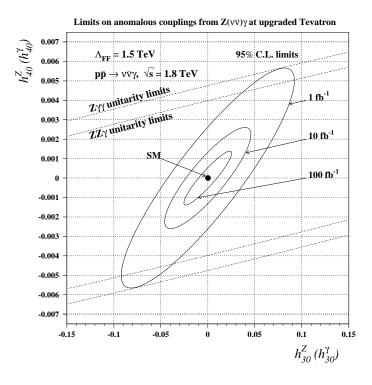


Figure 4.18: Projected 95% CL sensitivity limits for  $Z\gamma V$  couplings from  $Z\gamma$ ,  $Z\to \bar{\nu}\nu$  production at the Tevatron for integrated luminosities of 1 fb<sup>-1</sup>, 10 fb<sup>-1</sup> and 100 fb<sup>-1</sup>.

parton densities, and higher order QCD corrections was assumed to be 5%. From Fig. 4.17 one observes that the current limits on anomalous gauge boson couplings can be improved by about a factor 5 – 15 in  $W\gamma$  production if an integrated luminosity of 10 fb<sup>-1</sup> can be realized. Each additional factor 10 in integrated luminosity leads to roughly another factor 2 improvement in the sensitivities which can be achieved. Very similar results are obtained if DØ efficiencies and acceptances are used.

In Fig. 4.18 we show the limits on  $Z\gamma V$  couplings expected from  $p\bar{p} \to Z\gamma \to \bar{\nu}\nu\gamma$ , together with the constraints from unitarity, for a form factor scale of 1.5 TeV. The projected experimental limits for  $ZZ\gamma$  and  $Z\gamma\gamma$  couplings are virtually identical. The signal consists of a single high  $p_T$  photon accompanied by a large amount of missing transverse energy. Compared to the charged lepton decay modes of the Z boson, the decay  $Z \to \bar{\nu}\nu$  offers potential advantages. Due to the larger  $Z \to \bar{\nu}\nu$  branching ratio, the differential cross section is about a factor 3 larger than that for  $q\bar{q} \to e^+e^-\gamma$  and  $q\bar{q} \to \mu^+\mu^-\gamma$  combined. Furthermore, final state bremsstrahlung and timelike virtual photon diagrams do not contribute to the  $\bar{\nu}\nu\gamma$ final state. On the other hand, there are several potentially serious background processes which contribute to  $p\bar{p} \to \gamma p_T$ , but not to the  $\ell^+\ell^-\gamma$ ,  $\ell=e,\mu$  final state. The most important background processes are from  $W \to e\nu$  where the electron fakes a photon, cosmic muons, prompt photon production,  $p\bar{p} \to \gamma j$ , with the jet rapidity outside the range covered by the detector and thus "faking" missing transverse momentum, and two jet production where one of the jets is misidentified as a photon while the other disappears through the beam hole. To eliminate these backgrounds [66] as well as beam halo effects, we impose an  $E_T(\gamma)$ ,  $\not\!\!E_T > 40$  GeV cut and require the photon to be central. From Fig. 4.18 one observes that the present limits on  $Z\gamma V$  couplings from  $Z\gamma$  production with  $Z\to \ell^+\ell^-$  can be improved by a factor 50 - 200 (80 - 400) for an integrated luminosity of 1 fb<sup>-1</sup> (10 fb<sup>-1</sup>). The sensitivities expected from  $Z\gamma$  production with  $Z\to \ell^+\ell^-$ ,  $\ell=e,\,\mu$ , are about a factor 2 to 3 worse than those obtained from  $\bar{\nu}\nu\gamma$  production [67] (see Table 4.6). If the center of mass energy of the Tevatron can be increased to 2 TeV, slightly better limits than those shown in Fig. 4.18 can be obtained.

To estimate the sensitivity of  $W^+W^-$ ,  $W^{\pm}Z \to \ell\nu jj$  and  $WZ \to \ell^+\ell^- jj$ ,  $\ell=e,\mu$ , to non-standard WWV couplings in future Tevatron experiments, we require charged leptons to have  $E_T > 20 \text{ GeV}$  and  $|\eta(\ell)| < 2$ , and impose a missing transverse energy cut of 20 GeV. The two leading jets are required to have  $E_T(j) > 30 \text{ GeV}$  and  $60 \text{ GeV/c}^2 < m(jj) < 110 \text{ GeV/c}^2$ . Events containing an extra jet with  $E_T > 50$  GeV are vetoed in order to suppress the top quark background and to reduce the effect of QCD corrections [68, 69]. To suppress the W/Z+ jets background, a cut on the transverse momentum of the jet pair is imposed, similar to the requirement in the current CDF analysis. The value of the  $p_T(jj)$  cut varies with the integrated luminosity assumed:

$$p_T(jj) > 150 \text{ GeV/c}$$
 for  $\int \mathcal{L}dt = 100 \text{ pb}^{-1}$ , (4.46)

$$p_T(jj) > 200 \text{ GeV/c}$$
 for  $\int \mathcal{L}dt = 1 \text{ fb}^{-1}$ , (4.47)

$$p_T(jj) > 150 \text{ GeV/c}$$
 for  $\int \mathcal{L}dt = 100 \text{ pb}^{-1}$ , (4.46)  
 $p_T(jj) > 200 \text{ GeV/c}$  for  $\int \mathcal{L}dt = 1 \text{ fb}^{-1}$ , (4.47)  
 $p_T(jj) > 250 \text{ GeV/c}$  for  $\int \mathcal{L}dt = 10 \text{ fb}^{-1}$ . (4.48)

The number of signal events expected is calculated using the event generator of Ref. [70].

The trigger and particle identification efficiencies are assumed to be the same as in the current CDF data analysis. To estimate the  $t\bar{t}$  and W/Z+ jets background, ISAJET and VECBOS [71] are used. The top quark mass is taken to be  $M_{top}=170~{\rm GeV/c^2}$ .

Confidence levels are obtained by counting events above the  $p_T(jj)$  cut. The resulting 95% CL contours at  $\sqrt{s} = 1.8$  TeV for integrated luminosities of 100 pb<sup>-1</sup>, 1 fb<sup>-1</sup> and 10 fb<sup>-1</sup> are shown in Fig. 4.19a. To calculate the sensitivity limits in Fig. 4.19a, we have assumed a form factor scale of  $\Lambda_{FF} = 2$  TeV and the so-called "HISZ scenario" [67, 72], which reduces the number of independent WWV couplings from five to two. Choosing  $\Delta \kappa_{\gamma}$  and  $\lambda_{\gamma}$  as independent parameters, the WWZ couplings are then given by:

$$\Delta g_1^Z = \frac{1}{2\cos^2\theta_W} \Delta\kappa_\gamma, \tag{4.49}$$

$$\Delta \kappa_Z = \frac{1}{2} (1 - \tan^2 \theta_W) \, \Delta \kappa_\gamma, \tag{4.50}$$

$$\lambda_Z = \lambda_{\gamma}. \tag{4.51}$$

The sensitivity limits depend only marginally on the value of  $\Lambda_{FF}$  assumed. For different relations between anomalous couplings, similar bounds are obtained. The limits shown in Fig. 4.19a can be improved by 20 - 40% if a fit to the shape of the  $p_T(jj)$  distribution is performed.

With growing integrated luminosity, it is necessary to raise the  $p_T(jj)$  cut to eliminate the W/Z+ jets background. For increasing values of  $p_T(jj)$ , more and more jets tend to coalesce. As a result, the two jet reconstruction efficiency drops rapidly for  $p_T(jj) > 250 \text{ GeV/c}$ , and jet coalescing severely degrades the limits on anomalous WWV couplings which can be achieved for  $\int \mathcal{L}dt \geq 10 \text{ fb}^{-1}$ . WW and WZ production with all leptonic decays therefore may be more potent than the semihadronic channels in constraining the WWV vertices at very high luminosities.

In contrast to the WW,  $WZ \to \ell \nu jj$  and  $\ell^+\ell^- jj$  channels, double leptonic WZ decays are relatively background free and thus provide an excellent testing ground for non-standard WWZ couplings.  $WW \to \ell_1 \nu_1 \ell_2 \nu_2$  final states are plagued by background from  $t\bar{t}$  production, which, however, can be almost completely eliminated by either imposing a jet veto, or a cut on the hadronic transverse momentum in the event [63, 73]. Using recent calculations of  $W^{\pm}Z$  and WW production which include NLO QCD corrections [69, 73], sensitivity limits for the  $p\bar{p} \to W^{\pm}Z \to \ell_1^{\pm}\nu_1\ell_2^{+}\ell_2^{-}$ , and  $WW \to \ell_1^{\pm}\ell_2^{-}\not p_T$ ,  $\ell_{1,2}=e,\,\mu$ , channel were estimated. No full detector simulation was carried out, however, lepton identification cuts of  $p_T(\ell_{1,2}) > 20$  GeV/c and  $|\eta(\ell_{1,2})| < 2.5$ , and a missing  $p_T$  cut of 20 GeV/c (30 GeV/c) for WZ (WW) production have been imposed to roughly simulate detector response. Particle momenta are smeared according to the resolution of the CDF detector. The 95% CL limit contours for  $\sqrt{s}=1.8~{\rm TeV}$  and  $\Lambda_{FF}=1~{\rm TeV},$  obtained from a  $\chi^2$  fit to the  $p_T(Z)$ distribution for WZ production, and the  $p_T(\ell_1^+\ell_2^-)$  spectrum in the WW case, are displayed in Fig. 4.19b. Here we have again assumed the relations of Eqs. (4.49) - (4.51) for  $WW\gamma$ and WWZ couplings. If the center of mass energy of the Tevatron can be increased to 2 TeV, slightly better limits can be obtained. WZ production is seen to result in somewhat better limits on  $\Delta \kappa_{\gamma}^0$ , whereas the  $\ell_1^+\ell_2^-p_T$  final states are expected to yield more stringent

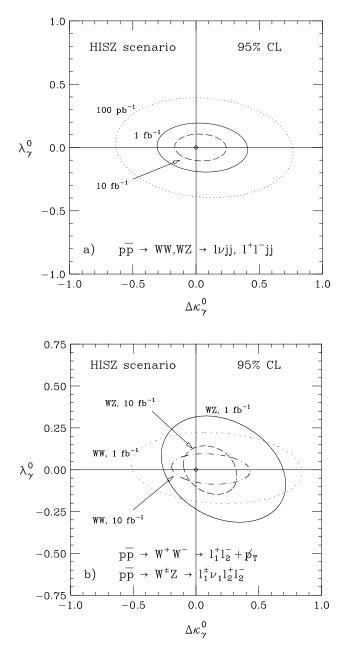


Figure 4.19: Expected 95% CL sensitivity limits for the WWV couplings in the HISZ scenario [see Eqs. (4.49) – (4.51)] a) from  $p\bar{p} \to WW, WZ \to \ell\nu jj$  and  $\ell^+\ell^- jj$ , and b) from  $p\bar{p} \to W^\pm Z \to \ell_1^\pm \nu_1 \ell_2^+ \ell_2^-$  and  $p\bar{p} \to W^+W^- \to \ell_1^+ \ell_2^- p_T$  for 1 fb<sup>-1</sup> and 10 fb<sup>-1</sup>.

bounds on  $\lambda_{\gamma}^{0}$ . For  $\int \mathcal{L}dt = 1$  fb<sup>-1</sup>, the small number of all leptonic events (see Table 4.1) severely limits the sensitivity, and the limits obtained from  $WW, WZ \to \ell \nu jj$  and  $\ell^{+}\ell^{-}jj$  are significantly better than those from double leptonic WZ and WW decays for most of the parameter space. For 10 fb<sup>-1</sup>, jet coalescing starts to negatively influence the semihadronic channels, and double leptonic and  $WW, WZ \to \ell \nu jj$  and  $\ell^{+}\ell^{-}jj$  final states yield comparable results. The contour limits shown in Figs. 4.17 and 4.19 depend only marginally on the form factor scale assumed; only the limits on the  $Z\gamma V$  couplings are more sensitive to the value of  $\Lambda_{FF}$  chosen.

The expected sensitivity bounds from future Tevatron experiments, varying only one of the independent couplings at a time, are summarized in Table 4.6. In order to demonstrate that the bounds obtained in the HISZ scenario are indeed representative, we also list the limits for  $W^{\pm}Z \to \ell_1^{\pm}\nu_1\ell_2^{+}\ell_2^{-}$  and  $W^{+}W^{-} \to \ell_1^{+}\nu_1\ell_2^{-}\nu_2$  in the case where each of the WWZ couplings is varied separately, with all other WWV couplings assuming their SM values. Future experiments at the Tevatron can measure  $\Delta \kappa_V$  and  $\Delta g_1^Z$  with a precision of about 0.1 - 0.2.  $\lambda_V$  can be determined to better than about 0.1 for  $\int \mathcal{L} dt \geq 1$  fb<sup>-1</sup>. The limits for  $Z\gamma V$  couplings are of order  $10^{-2} - 10^{-3}$ . While  $W\gamma$  production is seen to yield the best bounds at the Tevatron over a large fraction of the parameter space, it is clear that the limits obtained from the various processes are all of similar magnitude. Performing a global analysis of all di-boson production channels thus is expected to result in a significant improvement of the sensitivity bounds which can be achieved.

#### 4.7.4 Comparison with LEP II and LHC

In Fig. 4.20 we compare the limits expected from  $e^+e^- \to W^+W^- \to \ell\nu jj$ ,  $p\bar{p} \to W^\pm\gamma \to e^\pm\nu\gamma$ ,  $p\bar{p} \to W^\pm Z \to \ell_1^\pm\nu_1\ell_2^+\ell_2^-$  and  $p\bar{p} \to WW$ ,  $WZ \to \ell\nu jj$ ,  $\ell^+\ell^- jj$  in the HISZ scenario [see Eqs. (4.49) – (4.51)] for the envisioned energies and integrated luminosities of the Tevatron and LEP II. The limits expected for  $\Delta\kappa_{\gamma}$  are quite similar, whereas the Tevatron enjoys a clear advantage in constraining  $\lambda_{\gamma}$ , if correlations between the two couplings are taken into account. It should be noted, however, that the strategies to extract information on vector boson self-interactions at the two machines are very different. At the Tevatron one exploits the strong increase of the anomalous contributions to the helicity amplitudes with energy to derive limits. At LEP II, on the other hand, information is extracted from the angular distributions of the final state fermions. Data from the Tevatron and LEP II thus yield complementary information on the nature of the WWV couplings.

Because of the much higher energies accessible at the Tevatron and the steep increase of the anomalous contributions to the helicity amplitudes with energy, Tevatron experiments will be able to place significantly better limits (of  $\mathcal{O}(10^{-2}-10^{-3})$ ) on the  $Z\gamma V$  couplings than LEP II ( $\approx 0.5$ ) [67]. The Tevatron limits, however, do depend non-negligibly on the form factor scale assumed.

At the LHC, with 100 fb<sup>-1</sup>, one expects to probe anomalous WWV couplings with a precision of  $\mathcal{O}(10^{-1}-10^{-3})$  if the form factor scale  $\Lambda_{FF}$  is larger than about 2 TeV [67]. For  $\Delta \kappa_V$  ( $\lambda_V$ ) the limits expected at the LHC are about a factor 3 (10) better than those projected for the Tevatron with 10 fb<sup>-1</sup>. For  $Z\gamma V$  couplings, the LHC will yield limits which are a factor 10 to 100 better than those one hopes to achieve at the Tevatron, depending on

Table 4.6: Expected 95% CL limits on anomalous WWV,  $V=\gamma, Z$ , and  $ZZ\gamma$  couplings from future Tevatron experiments. Only one of the independent couplings is assumed to deviate from the SM at a time. The limits found for  $Z\gamma\gamma$  couplings are very similar to those obtained for  $h_3^Z$  and  $h_4^Z$ .

channel	limit	limit
	$\int \mathcal{L}dt = 1 \text{ fb}^{-1}$	$\int \mathcal{L}dt = 10 \text{ fb}^{-1}$
$p\bar{p} \to W^{\pm}\gamma \to e^{\pm}\nu\gamma$	$-0.38 < \Delta \kappa_{\gamma}^0 < 0.38$	$-0.21 < \Delta \kappa_{\gamma}^0 < 0.21$
$\sqrt{s} = 2 \text{ TeV}$	$-0.12 < \lambda_{\gamma}^{0} < 0.12$	$-0.057 < \lambda_{\gamma}^{0} < 0.057$
$p\bar{p} \to W^+W^-, W^{\pm}Z \to \ell^{\pm}\nu jj, \ell^+\ell^-jj$	$i -0.31 < \Delta \kappa_{\gamma}^0 < 0.41$	$-0.17 < \Delta \kappa_{\gamma}^0 < 0.24$
$\ell = e,  \mu,  \text{HISZ scenario}$	$-0.19 < \lambda_{\gamma}^0 < 0.19$	$-0.10 < \lambda_{\gamma}^0 < 0.11$
$p\bar{p} \to W^{\pm}Z \to \ell_1^{\pm}\nu_1\ell_2^{+}\ell_2^{-}$	$-0.26 < \Delta \kappa_{\gamma}^0 < 0.70$	$-0.09 < \Delta \kappa_{\gamma}^0 < 0.32$
$\ell_{1,2} = e, \mu, \text{HISZ scenario}$	$-0.24 < \lambda_{\gamma}^{0} < 0.32$	$-0.10 < \lambda_{\gamma}^0 < 0.13$
$p\bar{p} \to W^{\pm}Z \to \ell_1^{\pm}\nu_1\ell_2^{+}\ell_2^{-}$	$-0.78 < \Delta \kappa_Z^0 < 1.68$	$-0.33 < \Delta \kappa_Z^0 < 0.96$
$\ell_{1,2}=e,\mu$	$-0.24 < \lambda_Z^0 < 0.32$	$-0.10 < \lambda_Z^0 < 0.14$
	$-0.18 < \Delta g_1^{Z0} < 0.48$	$-0.06 < \Delta g_1^{Z0} < 0.22$
$p\bar{p} \to W^+W^- \to \ell_1^+ \nu_1 \ell_2^- \nu_2$	$-0.51 < \Delta \kappa_{\gamma}^0 < 0.84$	$-0.19 < \Delta \kappa_{\gamma}^0 < 0.43$
$\ell_{1,2} = e, \mu, \text{HISZ scenario}$	$-0.19 < \lambda_{\gamma}^0 < 0.22$	$-0.075 < \lambda_{\gamma}^{0} < 0.094$
$p\bar{p} \to W^+W^- \to \ell_1^+ \nu_1 \ell_2^- \nu_2$	$-0.44 < \Delta\kappa_Z^0 < 0.65$	$-0.17 < \Delta \kappa_Z^0 < 0.32$
$\ell_{1,2}=e,\mu$	$-0.24 < \lambda_Z^0 < 0.28$	$-0.10 < \lambda_Z^0 < 0.13$
SM $WW\gamma$ couplings	$-1.03 < \Delta g_1^{Z0} < 1.62$	$-0.45 < \Delta g_1^{Z0} < 0.83$
$p\bar{p} \to Z\gamma \to e^+e^-\gamma$	$-0.105 < h_{30}^Z < 0.105$	$-0.044 < h_{30}^Z < 0.044$
$\sqrt{s} = 2 \text{ TeV}, \Lambda_{FF} = 1.5 \text{ TeV}$	$-0.0064 < h_{40}^Z < 0.0064$	$-0.0025 < h_{40}^Z < 0.0025$
$p\bar{p} \to Z\gamma \to \bar{\nu}\nu\gamma$	$-0.038 < h_{30}^Z < 0.038$	$-0.024 < h_{30}^Z < 0.024$
$\sqrt{s} = 1.8 \text{ TeV}, \Lambda_{FF} = 1.5 \text{ TeV}$	$-0.0027 < h_{40}^Z < 0.0027$	$-0.0013 < h_{40}^Z < 0.0013$

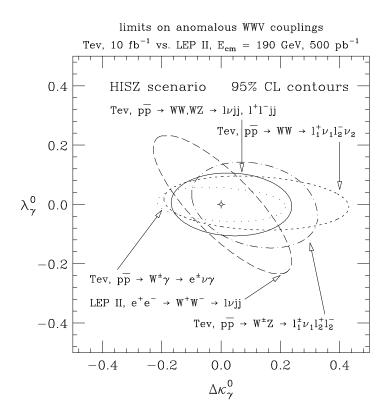


Figure 4.20: Comparison of the expected sensitivities on anomalous WWV couplings in the HISZ scenario from  $e^+e^- \to W^+W^- \to \ell\nu jj$  at LEP II and various processes at the Tevatron.

the form factor scale assumed [67].

# 4.7.5 Radiation Zero and Rapidity Correlations in $W\gamma$ Production

 $W\gamma$  production in hadronic collisions is of special interest due to the presence of a zero in the helicity amplitudes. It is well known that all SM helicity amplitudes of the parton-level subprocess  $q_1\bar{q}_2 \to W^{\pm}\gamma$  vanish for [74]

$$\cos \theta^* = \frac{Q_1 + Q_2}{Q_1 - Q_2} = \pm \frac{1}{3} , \qquad (4.52)$$

where  $\theta^*$  is the scattering angle of the W-boson with respect to the quark  $(q_1)$  direction in the  $W\gamma$  rest frame, and  $Q_i$  (i=1,2) are the quark charges in units of the proton electric charge e. This zero is a consequence of the factorizability of the amplitudes in gauge theories into one factor which contains the gauge coupling dependence and another which contains spin information. Although the factorization holds for any four-particle Born-level amplitude in which one or more of the four particles is a gauge-field quantum, the amplitudes for most processes may not necessarily develop a kinematical zero in the physical region. The

amplitude zero in the  $W^{\pm}\gamma$  process has been further shown to correspond to the absence of dipole radiation by colliding particles with the same charge-to-mass ratio [75], a realization of classical radiation interference and is therefore often referred to as the "radiation zero".

Non-standard  $WW\gamma$  couplings in general destroy the amplitude zero in  $W\gamma$  production. Searching for the radiation zero thus provides an additional powerful test of the gauge theory nature of the SM.

Unfortunately, the amplitude zero in  $q_1\bar{q}_2 \to W\gamma \to \ell\nu\gamma$  is not easy to observe in the  $\cos\theta^*$  distribution in pp or  $p\bar{p}$  collider experiments. Structure function effects transform the zero in the  $W\gamma$  case into a dip in the  $\cos\theta^*$  distribution. Higher order QCD corrections, finite W width effects, and photon radiation from the final state lepton line also tend to fill in the dip.

The main complication in the extraction of the  $\cos \theta^*$  distribution, however, originates from the finite resolution of the detector and ambiguities in reconstructing the parton center of mass frame. The ambiguities are associated with the nonobservation of the neutrino arising from W decay. Identifying the missing transverse momentum with the transverse momentum of the neutrino of a given  $W\gamma$  event, the unobservable longitudinal neutrino momentum,  $p_L(\nu)$ , and thus the parton center of mass frame, can be reconstructed by imposing the constraint that the neutrino and charged lepton four momenta combine to form the W rest mass. The resulting quadratic equation, in general, has two solutions. In the approximation of a zero W decay width, one of the two solutions coincides with the true  $p_L(\nu)$ . On an event by event basis, however, it is impossible to tell which of the two solutions is the correct one. This ambiguity considerably smears out the dip caused by the amplitude zero.

Instead of trying to reconstruct the parton center of mass frame and measure the  $\cos \theta^*$ or the equivalent rapidity distribution in the center of mass frame, one can study rapidity correlations between the observable final state particles in the laboratory frame. Knowledge of the neutrino longitudinal momentum is not required in determining this distribution. Event mis-reconstruction problems originating from the two possible solutions for  $p_L(\nu)$  are thus automatically avoided. In  $2 \to 2$  reactions differences of rapidities are invariant under boosts. One therefore expects that the double differential distribution of the rapidities,  $d^2\sigma/dy(\gamma)dy(W)$ , where y(W) and  $y(\gamma)$  are the W and photon rapidity, respectively, in the laboratory frame, exhibits a "valley" located at  $y(\gamma) - y(W) \approx -0.4$ , signaling the SM amplitude zero [76]. In  $W^{\pm}\gamma$  production, the dominant W helicity is  $\lambda_W = \pm 1$  [77], implying that the charged lepton,  $\ell = e, \mu$ , from  $W \to \ell \nu$  tends to be emitted in the direction of the parent W, and thus reflects most of its kinematic properties. As a result, the valley signaling the SM radiation zero should manifest itself also in the  $d^2\sigma/dy(\gamma)dy(\ell)$  distribution of the photon and lepton rapidities. The theoretical prediction of the  $d^2\sigma/dy(\gamma)dy(\ell)$  distribution in the Born approximation is shown in Fig. 4.21 and indeed exhibits a pronounced valley for rapidities satisfying  $\Delta y(\gamma, \ell) = y(\gamma) - y(\ell) \approx -0.3$ . To simulate detector response, transverse momentum cuts of  $p_T(\gamma) > 5 \text{ GeV/c}$ ,  $p_T(\ell) > 20 \text{ GeV/c}$  and  $p_T > 20 \text{ GeV/c}$ , rapidity cuts of  $|y(\gamma)| < 3$  and  $|y(\ell)| < 3.5$ , a cluster transverse mass cut of  $m_T(\ell\gamma; p_T) > 90 \text{ GeV/c}^2$ and a lepton photon separation cut of  $\Delta R(\gamma, \ell) > 0.7$  have been imposed. For 10 fb<sup>-1</sup>, a sufficient number of events should be available to map out  $d^2\sigma/dy(\gamma)dy(\ell)$ .

For smaller data sets, the rapidity difference distribution,  $d\sigma/d\Delta y(\gamma,\ell)$ , is a more useful

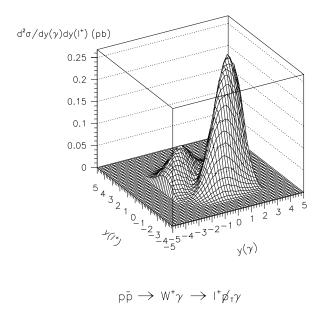


Figure 4.21: The double differential distribution  $d^2\sigma/dy(\gamma)dy(\ell)$  for  $p\bar{p}\to W^+\gamma\to\ell p_T\gamma$  at the Tevatron.

variable. In the photon lepton rapidity difference distribution, the SM radiation zero leads to a strong dip located at  $\Delta y(\gamma, \ell) \approx -0.3$  [76]. The LO and NLO predictions of the SM  $\Delta y(\gamma, \ell)$  differential cross section for  $p\bar{p} \to \ell^+ p_T \gamma$  at the Tevatron are shown in Fig. 4.22a.

Next-to-leading QCD corrections do not seriously affect the significance of the dip. However, a sufficient rapidity coverage is essential to observe the radiation zero in  $d^2\sigma/dy(\gamma)dy(\ell)$  and/or the  $\Delta y(\gamma,\ell)$  and distribution [76]. This is demonstrated in Fig. 4.23, which displays simulations of the rapidity difference distribution for 1 fb<sup>-1</sup> in the electron channel. If both central (|y| < 1.1) and endcap (1.5 < |y| < 2.5) electrons and photons can be used (Fig. 4.23a), the simulations indicate that with integrated luminosities  $\geq 1$  fb<sup>-1</sup> it will be possible to conclusively establish the dip in the photon lepton rapidity difference distribution which signals the presence of the radiation zero in  $W\gamma$  production. On the other hand, for central electrons and photons only, the dip is statistically not significant for 1 fb<sup>-1</sup>. With the detector upgrades currently planned for the Main Injector Era and beyond, both experiments should have the capability to analyze the  $\Delta y(\gamma,\ell)$  distribution over the full rapidity range of |y| < 2.5.

In pp collisions, the dip signaling the amplitude zero is shifted to  $\Delta y(\gamma, \ell) = 0$ . Because of the large qg luminosity, the inclusive QCD corrections are very large for  $W\gamma$  production at multi-TeV hadron colliders [78]. At the LHC, they enhance the cross section by a factor 2-3. The rapidity difference distribution for  $W^+\gamma$  production in the SM for pp collisions at  $\sqrt{s} = 14$  TeV is shown in Fig. 4.22b. Here we have imposed the following lepton and photon

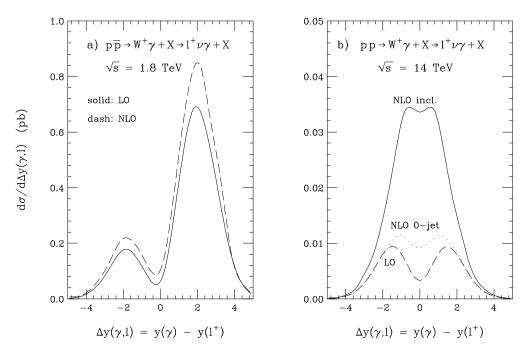


Figure 4.22: Photon lepton rapidity difference distribution for  $W\gamma$  production in the SM at a) the Tevatron and b) the LHC.

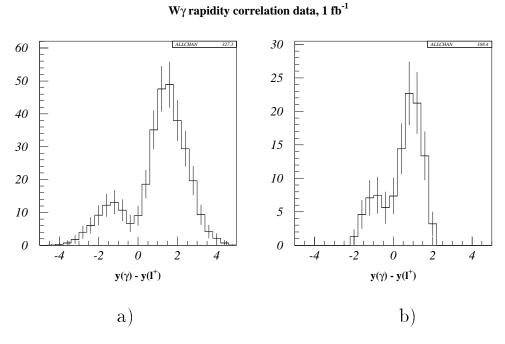


Figure 4.23: Simulation of the photon lepton rapidity difference distribution for  $W\gamma$  production for 1 fb<sup>-1</sup>, a) for central and endcap photons and electrons, b) for central electrons and photons only.

detection cuts:

$$p_T(\gamma) > 100 \text{ GeV/c}, \qquad |\eta(\gamma)| < 2.5,$$
 (4.53)

$$p_T(\ell) > 25 \text{ GeV/c}, \qquad |\eta(\ell)| < 3,$$
 (4.54)  
 $p_T > 50 \text{ GeV/c}, \qquad \Delta R(\gamma, \ell) > 0.7,$  (4.55)

$$p_T > 50 \text{ GeV/c}, \qquad \Delta R(\gamma, \ell) > 0.7, \qquad (4.55)$$

The inclusive NLO QCD corrections are seen to considerably obscure the amplitude zero. The bulk of the corrections at LHC energies originates from quark gluon fusion and the kinematical region where the photon is produced at large  $p_T$  and recoils against a quark, which radiates a soft W boson which is almost collinear to the quark. Events which originate from this phase space region usually contain a high  $p_T$  jet. A jet veto therefore helps to reduce the QCD corrections. Nevertheless, the remaining QCD corrections still substantially reduce the visibility of the radiation zero in  $W\gamma$  production at the LHC [76].

Given a sufficiently large integrated luminosity, experiments at the Tevatron studying lepton photon rapidity correlations therefore offer a unique chance to observe the SM radiation zero in  $W\gamma$  production.

Indirectly, the radiation zero can also be observed in the  $Z\gamma$  to  $W\gamma$  cross section ratio [79]. Many theoretical and experimental uncertainties at least partially cancel in the cross section ratio. On the other hand, in searching for the effects of the SM radiation zero in the  $Z\gamma$  to  $W\gamma$  cross section ratio, one has to assume that the SM is valid for  $Z\gamma$  production. Since the radiation zero occurs at a large scattering angle, the photon  $E_T$  distribution in  $W\gamma$  production falls much more rapidly than that of photons in  $Z\gamma$  production. As a result, the SM  $W\gamma$  to  $Z\gamma$  event ratio,  $N_{W\gamma}/N_{Z\gamma}$ , as a function of the photon transverse energy,  $E_T^{\gamma}$ , drops rapidly. As demonstrated in Fig. 4.24 for the electron channel, the event ratio can be mapped out to  $E_T^{\gamma} \approx 200 \text{ GeV}$  with 10 fb<sup>-1</sup>, thus making it possible to conclusively establish the rapid drop in the event ratio predicted by the SM (solid line). From a comparison of the observed cross section ratio with the SM prediction, one can in principle also extract limits on anomalous  $WW\gamma$  and  $Z\gamma V$  couplings.

#### 4.7.6Probing QCD in $W\gamma$ Production

For an integrated luminosity of 10 fb<sup>-1</sup>, one expects approximately 5,000  $W^{\pm}\gamma$ ,  $W \rightarrow e\nu$ events. Besides detailed tests of the  $WW\gamma$  couplings the large data sample expected will make it possible to measure a number of interesting observables, such as the  $p_T$  distribution of the  $W\gamma$  pair. Similar to the transverse momentum distribution of the W and Z bosons [80], a measurement of the  $W\gamma$   $p_T$  spectrum constitutes an excellent test of QCD. In the small transverse momentum region, soft gluon resummation, and non-perturbative QCD effects are probed [81]. Perturbative QCD is tested for  $p_T(W\gamma) > 40 \text{ GeV/c}$ . Presently, only a calculation of  $W\gamma$  production at NLO in QCD exits; resummation effects have not yet been included in the theoretical predictions.

At large  $W\gamma$  transverse momenta, QCD predicts a collinear enhancement factor in the  $qq \to W\gamma q'$  partonic cross section [78]. It arises from the kinematical region where the photon recoils against a quark jet, which radiates a soft W boson which is almost collinear to the quark. QCD corrections therefore change the shape of the photon transverse

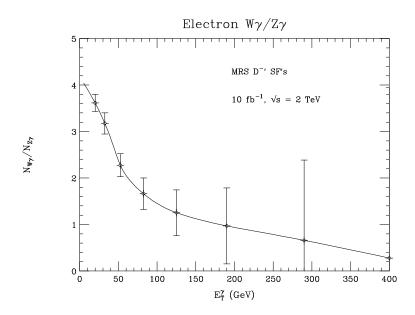


Figure 4.24:  $W\gamma$  to  $Z\gamma$  cross section ratio. The solid line is the SM prediction.

momentum distribution, and lead to a rather hard  $p_T(W\gamma)$  distribution in the region above 40 GeV/c, where the  $W\gamma$  transverse momentum spectrum is dominated by the contribution from  $W\gamma + 1$  jet production.

The effect of the collinear enhancement factor on the  $p_T(W\gamma)$  distribution in the perturbative region is illustrated in Fig. 4.25. The solid line displays the lowest order QCD prediction from the calculation of Ref. [78]. The dashed line, on the other hand, shows the  $W\gamma$  transverse momentum distribution one would expect, if the shape of the  $W\gamma$   $p_T$  distribution and the W transverse momentum distribution would be identical. To obtain the dashed line,  $W\gamma$  events were generated using the leading (Born) order calculation of Ref. [82], and boosting the  $W\gamma$  system in the transverse plane according to the W transverse momentum distribution measured by CDF in the 1988-89 run [83]. The measured  $p_T(W)$  distribution was found to agree very well with the QCD prediction [84] in the perturbative region. The normalization of the dashed line was adjusted by multiplying the LO  $W\gamma$  cross section within cuts by the ratio of NLO to LO cross sections (k-factor). Identical cuts ( $E_T(\gamma) > 10$  GeV,  $E_T(e)$ ,  $E_T > 20$  GeV,  $\Delta R(e, \gamma) > 0.7$ ,  $|\eta(\gamma)|$ ,  $|\eta(e)| < 2.5$ ,  $m_T(e\gamma; E_T) > 90$  GeV/c<sup>2</sup>, standard photon isolation) and parameters have been used to obtain the two curves.

Figure 4.25 shows that the shape of the  $W\gamma$  transverse momentum distribution predicted by QCD is significantly harder than that of the  $p_T(W)$  spectrum. The error bars in Fig. 4.25 indicate the expected statistical uncertainties for an integrated luminosity of 10 fb<sup>-1</sup>. The size of the error bars shows that, with 10 fb<sup>-1</sup>, it should be feasible to map out the  $p_T(W\gamma)$ distribution to transverse momenta in excess of 100 GeV and to discriminate between the two distributions approximately at the  $7\sigma$  level.

A similar measurement can be carried out for  $Z\gamma$  production, although the significantly smaller number of events limits the accessible  $p_T$  range.

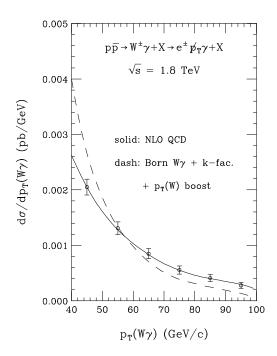


Figure 4.25:  $W\gamma$  transverse momentum distribution at the Tevatron in the perturbative region. The solid curve shows the distribution predicted by QCD at  $\mathcal{O}(\alpha_s)$ . The dashed line displays the distribution one would expect if the shape of the W and  $W\gamma$  transverse momentum would be identical. The error bars indicate the statistical uncertainties expected for an integrated luminosity of 10 fb<sup>-1</sup>.

### 4.8 Triple Gauge Boson Production

The very large integrated luminosities expected in future Tevatron runs offer also the possibility to search for triple vector boson production and thus to probe the quartic boson self-interactions ( $WW\gamma\gamma$ , WWZZ etc.). The triple vector boson production processes can be classified according to the number of photons in the final state:

$$p\bar{p} \rightarrow \gamma\gamma\gamma,$$
 (4.56)

$$p\bar{p} \rightarrow W^{\pm}\gamma\gamma, Z\gamma\gamma,$$
 (4.57)

$$p\bar{p} \rightarrow W^+W^-\gamma, W^{\pm}Z\gamma, ZZ\gamma,$$
 (4.58)

$$p\bar{p} \to W^+W^-W^{\pm}, W^+W^-Z, W^{\pm}ZZ, ZZZ.$$
 (4.59)

We will not consider the pure QED process  $p\bar{p} \to \gamma\gamma\gamma$  here. Since top quarks decay almost exclusively into Wb, the  $W^+W^-V$ ,  $V=W^\pm$ ,  $\gamma$ , Z channels also receive contributions from  $t\bar{t}V$  production. For a top quark mass of 175 GeV/c², the  $t\bar{t}V$  and  $W^+W^-V$  production cross sections are very similar at the Tevatron. The b-quarks produced in top quark decays frequently lead to one or two hadronic jets. The jet activity of WWV events may therefore be used to separate the WWV and  $t\bar{t}V$  processes. Higgs boson exchange contributes to the processes listed in Eq. (4.59) and enhances the cross section by up to a factor 6.

Table 4.7: Triple gauge boson production cross sections at the Tevatron ( $\sqrt{s} = 2$  TeV) for  $M_{top} = 175 \text{ GeV/c}^2$  and  $M_H = 100 \text{ GeV/c}^2$ . The branching ratios of the leptonic W and Z decays with  $\ell = e$ ,  $\mu$  are included in the cross section listed.

channel	cross section (fb)
$W^{\pm}\gamma\gamma \to \ell^{\pm}\nu\gamma\gamma,  p_T(\gamma) > 10 \text{ GeV},   \eta(\gamma)  < 2.5$	4.6
$Z\gamma\gamma \to \ell^+\ell^-\gamma\gamma,  p_T(\gamma) > 10 \text{ GeV},   \eta(\gamma)  < 2.5$	3.2
$W^{+}W^{-}\gamma \to \ell_{1}^{+}\nu_{1}\ell_{2}^{-}\bar{\nu}_{2}\gamma, \ p_{T}(\gamma) > 10 \text{ GeV}, \  \eta(\gamma)  < 2.5$ $t\bar{t}\gamma \to W^{+}W^{-}\gamma \to \ell_{1}^{+}\nu_{1}\ell_{2}^{-}\bar{\nu}_{2}\gamma, \ p_{T}(\gamma) > 10 \text{ GeV}, \  \eta(\gamma)  < 2.5$	2.0 1.7
$W^{\pm}Z\gamma \to \ell_1^{\pm}\nu_1\ell_2^{+}\ell_2^{-}\gamma,  p_T(\gamma) > 10 \text{ GeV},   \eta(\gamma)  < 2.5$	0.12
$ZZ\gamma \to \ell^+\ell^-\bar{\nu}\nu\gamma,  p_T(\gamma) > 10 \text{ GeV},   \eta(\gamma)  < 2.5$	0.18
$ZZ\gamma \to \ell_1^+ \ell_1^- \ell_2^+ \ell_2^- \gamma, \ p_T(\gamma) > 10 \text{ GeV}, \  \eta(\gamma)  < 2.5$	0.03
$W^{+}W^{-}W^{\pm} \to \ell_{1}^{+}\nu_{1}\ell_{2}^{-}\nu_{2}\ell_{3}^{\pm}\nu_{3}$ $t\bar{t}W^{\pm} \to W^{+}W^{-}W^{\pm} \to \ell_{1}^{+}\nu_{1}\ell_{2}^{-}\nu_{2}\ell_{3}^{\pm}\nu_{3}$	$0.06 \\ 0.05$
$W^{+}W^{-}Z \to \ell_{1}^{+}\nu_{1}\ell_{2}^{-}\nu_{2}\ell_{3}^{+}\ell_{3}^{-}$ $t\bar{t}Z \to W^{+}W^{-}Z \to \ell_{1}^{+}\nu_{1}\ell_{2}^{-}\nu_{2}\ell_{3}^{+}\ell_{3}^{-}$	0.02 0.01
$W^{\pm}ZZ \to \ell_1^{\pm} \nu_1 \ell_2^{+} \ell_2^{-} \ell_3^{+} \ell_3^{-}$	$1.1 \cdot 10^{-3}$
$ZZZ \to \ell_1^+ \ell_1^- \ell_2^+ \ell_2^- \bar{\nu}\nu$	$1.3\cdot 10^{-3}$
$ZZZ \to \ell_1^+ \ell_1^- \ell_2^+ \ell_2^- \ell_3^+ \ell_3^-$	$1.5 \cdot 10^{-4}$

The cross sections for the triple gauge boson production processes at the Tevatron are listed in Table 4.7 [5]. For an integrated luminosity of 10 fb<sup>-1</sup>, a sufficient number of  $W\gamma\gamma$ ,  $Z\gamma\gamma$  and  $WW\gamma$  events should be observed to extract information on the quartic gauge boson couplings. For all other processes one expects at most a few candidate events, unless the quartic couplings substantially deviate from the SM prediction.

#### 4.9 Conclusions

With very large integrated luminosities at the Tevatron, the electroweak sector sector of the SM can be probed in great detail. From our partly preliminary studies we arrive at the following conclusions:

• With 10 fb<sup>-1</sup> it should be possible to measure the mass of the W boson with a precision of at least 30 MeV/c<sup>2</sup>. An uncertainty of 20 MeV/c<sup>2</sup> may well be within reach. This

is about a factor of 2 better than what one expects for LEP II. With a precision of 20  $\text{MeV/c}^2$  (30  $\text{MeV/c}^2$ ) for the W mass, and 2  $\text{GeV/c}^2$  for the top quark mass, the Higgs Boson mass can be predicted with an uncertainty of about 40% (50%). Comparison with the results of a direct search at the Tevatron and LHC may constitute the ultimate test of the SM.

- The W width can be measured with an uncertainty of about 15 MeV. This is an improvement of almost one order of magnitude of the current uncertainty. At LEP II  $\Gamma_W$  can only be measured with a precision of a few hundred MeV.
- The W charge asymmetry will be a very powerful tool in constraining the parton distribution functions. In many processes the error in the parton distribution functions currently constitutes a major source of uncertainty. The forward backward asymmetry,  $A_{FB}$  in Z boson decays provides a useful cross check on the Higgs boson mass extracted from the W mass measurement.
- With an integrated luminosity of 10 fb<sup>-1</sup>, limits on the branching ratios of rare W decays of  $\mathcal{O}(10^{-5})$  to  $\mathcal{O}(10^{-7})$  can be obtained. W decays into two pseudoscalar mesons offer an opportunity to probe meson decay form factors at a very high momentum transfer where these form factors have not been tested so far.
- The Tevatron offers a unique opportunity to search for CP violation in W boson production and decay since it collides protons and antiprotons, ie. the initial state is a CP eigenstate. The extremely large number of W boson events expected at a superluminous Tevatron will make it possible to search for small CP-violating contributions to W boson production, at the level of  $\mathcal{O}(10^{-3} 10^{-4})$ .
- With 10 fb<sup>-1</sup>, the WWV and  $Z\gamma V$ ,  $V=\gamma$ , Z, vertices can be determined with a precision of  $\mathcal{O}(10\%)$  and  $\mathcal{O}(10^{-2}-10^{-3})$ , respectively, at the Tevatron. The expected accuracy for the WWV couplings is comparable or better than that of LEP II. However, since the methods used to extract limits on anomalous couplings at the two colliders are different, data from the Tevatron and LEP II yield complementary information. Tevatron experiments will be able to place limits on the  $Z\gamma V$  couplings which are up to a factor 100 better than those which can be achieved at LEP II. At the LHC, with 100 fb<sup>-1</sup>, it will be possible to place limits on anomalous WWV and  $Z\gamma V$  couplings which are a factor 3 to 100 better than those one can expect for the Tevatron with 10 fb<sup>-1</sup>.
- The Tevatron offers a unique chance to search for the SM "radiation zero" in  $W\gamma$  production, which provides an additional powerful test of the gauge theory nature of the SM. At the LHC, due to the large qg luminosity, QCD corrections obscure the dip in the photon lepton rapidity difference distribution which is caused by the radiation zero. This is not the case at Tevatron energies. Currently, the experimental results are statistically limited. With integrated luminosities of 2 fb<sup>-1</sup> or more, it should be possible to conclusively establish the existence of the radiation zero.
- A superluminous Tevatron will make it possible to obtain direct information on the quartic vector boson couplings. For an integrated luminosity of 10 fb<sup>-1</sup>, a sufficient

number of  $W\gamma\gamma$ ,  $Z\gamma\gamma$  and  $WW\gamma$  events should be observed to extract information on the quartic gauge boson couplings.

#### ${\bf Acknowledgements}$

We would like to thank W. Bardeen, G. Burdman, E. Eichten, K. Einsweiler, W. Giele, C. Hill and P. Tipton for stimulating discussions.

## **Bibliography**

- [1] P. Renton, OUNP-95-20 (preprint, October 1995), to appear in the Proceedings of the International Symposium on Lepton Photon Interactions, Beijing, August 1995.
- [2] D. Schaile, CERN-PPE/94-162 (preprint, October 1994), in Proceedings of the "27th International Conference on High Energy Physics", Glasgow, Scotland, July 1994, Vol. I, p. 27; The LEP Collaborations, CERN-PPE/94-187 (preprint, November 1994).
- [3] G. Jackson, Recycler Ring Conceptual Design Study, FERMILAB-TM-1936 (July 1995).
- [4] S. Dawson and G. Valencia, Phys. Rev. **D52**, 2717 (1995).
- [5] T. Han and R. Sobey, UCD-95-22 (preprint, July 1995).
- [6] S. Godfrey, Proceedings of the "International Symposium of Vector Boson Self Interactions", Los Angeles, CA, February 1995, p. 209.
- [7] F. Abe et al. (CDF Collaboration), Phys. Rev. Lett. 75, 11 (1995) and Phys. Rev. D52, 4784 (1995).
- [8] U. Baur and D. Zeppenfeld, Phys. Rev. Lett. 75, 1002 (1995).
- [9] V. Khoze and W.J. Stirling, Phys. Lett. B356, 373 (1995); V. Khoze and T. Sjostrand, DTP/95/68 (preprint, August 1995).
- [10] C. Balázs, J. Qiu and C.P. Yuan, Phys. Lett. **B355**, 548 (1995).
- [11] M.H. Reno, Phys. Rev. **D49**, 4326 (1994).
- [12] W. Carithers, TEV2000 workshop note (October 1994).
- [13] A. Peryshkin, Proceedings of the Workshop on Physics at Current Accelerators and the Supercollider, Argonne, June 1993, p. 295.
- [14] M. Austern and R. Cahn, LBL-33780, April 1993; H.S. Chen and G.J. Zhou, Phys. Lett. B331, 441 (1994); W.J. Stirling, DTP/95/24 (preprint, February 1995).
- [15] P. Perez, DAPNIA/SPP 95-21 (preprint, October 1995), to appear in the Proceedings of the International Europhysics Conference on High Energy Physics, Brussels, Belgium, July 27 – August 2, 1995.

- [16] D. Gingrich et al. (ATLAS Collaboration), ATLAS Letter of Intent, CERN-LHCC-92-4 (October 1992); W. W. Armstrong et al. (ATLAS Collaboration), ATLAS Technical Design Report, CERN-LHCC-94-43 (December 1994).
- [17] M. Della Negra et al. (CMS Collaboration), CMS Letter of Intent, CERN-LHCC-92-3 (October 1992); G. L. Bayatian et al. (CMS Collaboration), CMS Technical Design Report, CERN-LHCC-94-38 (December 1994).
- [18] K. Einsweiler, private communication.
- [19] F. Halzen, B. Kniehl, and M.L. Stong, Z. Phys. C58, 119 (1993); F. Halzen and B. Kniehl, Nucl. Phys. B353, 567 (1990).
- [20] F. Merritt, H. Montgomery, A. Sirlin and M. Swartz, "Precision Tests of Electroweak Physics", in "Particle Physics Perspectives and Opportunities, Report of the DPF Committee on Long Term Planning", eds. R.D. Peccei et al., p. 19.
- [21] H. Burkhardt and B. Pietrzyk, Phys. Lett. **B356**, 398 (1995); S. Eidelmann and F. Jegerlehner, Z. Phys. **C67**, 585 (1995); R.B.Nevzorov, A.V. Novikov and M.I. Vysotsky, JETP Lett. **60**, 399 (1994); A.D. Martin and D. Zeppenfeld, Phys. Lett. **B345**, 558 (1995); M. Swartz, SLAC-PUB-95-7001 (preprint, September 1995).
- [22] F. Abe et al. (CDF Collaboration), Phys. Rev. Lett. 74, 341 (1995).
- [23] F. Abe et al. (CDF Collaboration), Phys. Rev. Lett. 73, 220 (1994) and Phys. Rev. D52, 2624 (1995); S. Abachi et al. (DØ Collaboration), Phys. Rev. Lett. 75, 1456 (1995).
- [24] J. Rosner, M. Worah and T. Takeuchi, Phys. Rev. **D49**, 1363 (1994).
- [25] M. Swartz, SLAC-PUB-5258 (June 1990).
- [26] F. Nang (DØ Collaboration), Proceedings of the "DPF94 Conference", Albuquerque, NM, August 1994, pp. 1644; W. Giele, E.W.N. Glover and D. Kosower, Phys. Rev. D52, 1486 (1995); S.D. Ellis and D.E. Soper, Phys. Rev. Lett. 74, 5182 (1995).
- [27] E. Kovacs (CDF Collaboration), Proceedings of the "DPF94 Conference", Albuquerque, NM, August 1994, p. 1653; W. Giele, E.W.N. Glover and D. Kosower, Phys. Lett. **B339**, 181 (1994).
- [28] A.D. Martin, R.G. Roberts and W.J. Stirling, Mod. Phys. Lett. A4, 1135 (1989);
   E.L. Berger et al., Phys. Rev. D40, 83 (1989).
- [29] F. Abe et al. (CDF Collaboration), Phys. Rev. Lett. 74, 850 (1995).
- [30] H.L. Lai et al., (CTEQ Collaboration), Phys. Rev. **D51**, 4763 (1995); A.D. Martin,
   R.G. Roberts and W.J. Stirling, Phys Rev. **D50**, 6734 (1994).
- [31] J.L. Rosner, Phys. Lett. **B221**, 85 (1989).

- [32] F. Abe et al. (CDF Collaboration), Phys. Rev. Lett. 67, 1502 (1991).
- [33] P. Fisher, U. Becker and P. Kirkby, Phys. Lett. **B356**, 404 (1995).
- [34] M. Schmelling, CERN-PPE/95-129 (preprint, August 1995), to appear in the Proceedings of the "XV International Conference on Physics in Collision", Cracow, Poland, June, 1995; P. Langacker and N. Polonsky, Phys. Rev. D52, 3081 (1995).
- [35] W. Giele, E.W.N. Glover and J. Yu, FERMILAB-Pub-95/127-T (preprint, July 1995).
- [36] C. Balazs and C.P. Yuan, in preparation.
- [37] A.D. Martin, R.G. Roberts and W.J. Stirling, Phys. Lett. **B356**, 89 (1995); CTEQ Collaboration, in preparation.
- [38] P. Arnold and M.H. Reno, Nucl. Phys. B319, 37 (1989); (E) B330, 284 (1990);
   P. Arnold, R.K. Ellis and M.H. Reno, Phys. Rev. D40, 912 (1989).
- [39] F. Abe et al. (CDF Collaboration), Phys. Rev. Lett. 67, 2938 (1991); S. Abachi et al. (DØ Collaboration), FERMILAB-Conf-95/259-E (preprint, August 1995), contributed paper to the Europhysics Conference on High Energy Physics, Brussels, Belgium, July 27 August 2, 1995.
- [40] F. Abe et al. (CDF Collaboration), FERMILAB-Pub-95/301-E (preprint, September 1995), submitted to Phys. Rev. Lett.
- [41] W. Bernreuther et al., in "Z Physics at LEP I", CERN 89-08, 1989 (Yellow Report), Vol. 2, p. 1.
- [42] F. Abe et al. (CDF Collaboration), Phys. Rev. Lett. 69, 2160 (1992); S. Kopp, FERMILAB-Pub-95/264-E (preprint, August 1995), to appear in Int. J. Mod. Phys. A; F. Abe, et al. (CDF Collaboration), to be submitted (Oct. 1995) to Phys. Rev. Lett. See also J. Alitti, et al. (UA2 Collaboration), Phys. Lett. B277, 203 (1992).
- [43] C. Albajar et al. (UA1 Collaboration), Phys. Lett **B241**, 283 (1990); J. Alitti et al. (UA2 Collaboration), Phys. Lett **B277**, 203 (1992).
- [44] L. Arnellos, W.J. Marciano and Z. Parsa, Nucl. Phys. **B196**, 378 (1982).
- [45] G.P. Lepage and S.J. Brodsky, Phys. Lett. B87, 359 (1979); A. Duncan and A. Mueller, Phys. Rev. D21, 1636 (1980).
- [46] J. Richman and P. Burchat, UCSB-HEP-95-08, to appear in Rev. Mod. Phys.
- [47] E. Eichten and C. Quigg, Phys. Rev. **D49**, 5845 (1994).
- [48] L. Montanet et al. (Particle Data Group), Phys. Rev. **D50**, 1173 (1994).
- [49] G. Burdman, private communication.
- [50] R. Barbieri, A. Georges and P. Le Doussal, Z. Phys. C32, 437 (1986).

- [51] A. Brandenburg, J. Ma, R. Munch, and O. Nachtmann, Z. Phys. C51, 225 (1991).
- [52] A. Brandenburg, J. Ma, and O. Nachtmann, Z. Phys. C55, 115 (1992).
- [53] P. Chiappetta and M. Le Bellac, Z. Phys. C32, 521 (1986).
- [54] K. Hagiwara, K. Hikasa, R. D. Peccei, D. Zeppenfeld, Nucl. Phys. B282, 253 (1987);
   K. Gaemers and G. Gounaris, Z. Phys. C1, 259 (1979).
- [55] H. Aronson, Phys. Rev. 186, 1434 (1969); K. J. Kim and Y.-S. Tsai, Phys. Rev. D7, 3710 (1973).
- [56] U. Baur and D. Zeppenfeld, Phys. Lett. **B201**, 383 (1988).
- [57] F. Abe et al. (CDF Collaboration), Phys. Rev. Lett. **74**, 1936 (1995).
- [58] S. Abachi et al. (DØ Collaboration), Phys. Rev. Lett. **75**, 1034 (1995).
- [59] D. Benjamin, FERMILAB-Conf-95/241-E (June 1995), to appear in the Proceedings of the "10th Topical Workshop on Proton Antiproton Collider Physics", Fermilab, May 1995.
- [60] F. Abe et al. (CDF Collaboration), Phys. Rev. Lett. 74, 1941 (1995).
- [61] S. Abachi et al. (DØ Collaboration), Phys. Rev. Lett. **75**, 1028 (1995).
- [62] F. Abe et al. (CDF Collaboration), Phys. Rev. Lett. 75, 1018 (1995).
- [63] S. Abachi et al. (DØ Collaboration), Phys. Rev. Lett. **75**, 1024 (1995).
- [64] S. Abachi *et al.* (DØ Collaboration), FERMILAB-Conf-95/250-E (July 1995), contributed paper to the Europhysics Conference on High Energy Physics, Brussels, 27 July 2 August 1995.
- [65] M. Acciarri et al. (L3 Collaboration), Phys. Lett. **B346**, 190 (1995).
- [66] U. Baur and E. L. Berger, Phys. Rev. **D47**, 4889 (1993).
- [67] H. Aihara et al., Summary of the Working Subgroup on Anomalous Gauge Boson Interactions of the DPF Long Range Planning Study, FERMILAB-Pub-95/031, March 1995, preprint, to appear in "Electroweak Symmetry Breaking and New Physics at the TeV Scale", eds. T. Barklow, S. Dawson, H. Haber and J. Siegrist.
- [68] J. Ohnemus, Phys. Rev. **D44**, 1403 (1991); Phys. Rev. **D44**, 3477 (1991); Phys. Rev. **D50**, 1931 (1994); J. Ohnemus and J. Owens, Phys. Rev. **D43**, 3626 (1991); S. Frixione, Nucl. Phys. **B410**, 280 (1993); S. Frixione, P. Nason, and S. Ridolfi, Nucl. Phys. **B383**, 3 (1992).
- [69] U. Baur, J. Ohnemus, and T. Han, Phys. Rev. **D51**, 3381 (1995).
- [70] K. Hagiwara, J. Woodside, and D. Zeppenfeld, Phys. Rev. **D41**, 2113 (1990).

- [71] F. A. Berends et al., Nucl. Phys. **B357**, 32 (1991).
- [72] K. Hagiwara, S. Ishihara, R. Szalapski, and D. Zeppenfeld, Phys. Lett. B283, 353 (1992), and Phys. Rev. D48, 2182 (1993).
- [73] U. Baur, J. Ohnemus, and T. Han, UCD-95-21 (preprint, July 1995), to appear in Phys. Rev. **D**.
- [74] R. W. Brown et al., Phys. Rev. D20, 1164 (1979); K. O. Mikaelian et al., Phys. Rev. Lett. 43, 746 (1979).
- [75] S. J. Brodsky and R. W. Brown, Phys. Rev. Lett. 49, 966 (1982); R. W. Brown et al., Phys. Rev. D28, 624 (1983); R. W. Brown and K. L. Kowalski, Phys. Rev. D29, 2100 (1984).
- [76] U. Baur, S. Errede, and G. Landsberg, Phys. Rev. **D50**, 1917 (1994).
- [77] C. Bilchak, R. Brown, and J. Stroughair, Phys. Rev. **D29**, 375 (1984).
- [78] U. Baur, T. Han, and J. Ohnemus, Phys. Rev. **D48**, 5140 (1993).
- [79] U. Baur, S. Errede, and J. Ohnemus, Phys. Rev. **D48**, 4103 (1993).
- [80] C. Albajar et al. (UA1 Collaboration), Z. Phys. C44, 15 (1989); J. Alitti et al. (UA2 Collaboration), Z. Phys. 47, 523 (1990); F. Abe et al. (CDF Collaboration); Phys. Lett. 66, 2951 (1991); Phys. Lett. 67, 2938 (1991); S. Abachi et al. (DØ Collaboration), FERMILAB-Conf-95/259-E (August 1995), contributed paper to the International Europhysics Conference on High Energy Physics, Brussels, Belgium, 27 July 2 August, 1995.
- [81] G. Ladinsky and C.P. Yuan, Phys. Rev. **D50**, 4239 (1994).
- [82] U. Baur and E. L. Berger, Phys. Rev. **D41**, 1476 (1990).
- [83] F. Abe et al. (CDF Collaboration); Phys. Lett. 66, 2951 (1991).
- [84] P. Arnold and R. Kauffman, Nucl. Phys. **B349**, 381 (1991).